

Structure- and Reactivity-Based Development of Covalent Inhibitors of the Activating and Gatekeeper Mutant Forms of the Epidermal Growth Factor Receptor (EGFR)

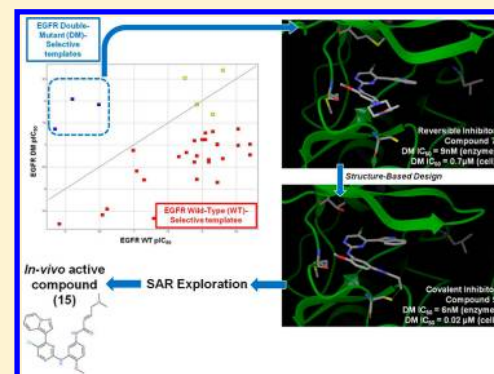
Richard A. Ward,* Mark J. Anderton, Susan Ashton, Paul A. Bethel, Matthew Box, Sam Butterworth, Nicola Colclough, Christopher G. Chorley, Claudio Chuaqui,[†] Darren A. E. Cross, Les A. Dakin,[†] Judit É. Debreczeni, Cath Eberlein, M. Raymond V. Finlay, George B. Hill, Matthew Grist, Teresa C. M. Klinowska, Clare Lane, Scott Martin, Jonathon P. Orme, Peter Smith,[‡] Fengjiang Wang,[†] and Michael J. Waring

AstraZeneca, Oncology & Discovery Sciences Innovative Medicines, Mereside, Alderley Park, Macclesfield, Cheshire SK10 4TG, United Kingdom

[†]AstraZeneca, Oncology Innovative Medicines, Gatehouse Park, Waltham, Massachusetts 02451, United States

S Supporting Information

ABSTRACT: A novel series of small-molecule inhibitors has been developed to target the double mutant form of the epidermal growth factor receptor (EGFR) tyrosine kinase, which is resistant to treatment with gefitinib and erlotinib. Our reported compounds also show selectivity over wild-type EGFR. Guided by molecular modeling, this series was evolved to target a cysteine residue in the ATP binding site via covalent bond formation and demonstrates high levels of activity in cellular models of the double mutant form of EGFR. In addition, these compounds show significant activity against the activating mutations, which gefitinib and erlotinib target and inhibition of which gives rise to their observed clinical efficacy. A glutathione (GSH)-based assay was used to measure thiol reactivity toward the electrophilic functionality of the inhibitor series, enabling both the identification of a suitable reactivity window for their potency and the development of a reactivity quantitative structure-property relationship (QSPR) to support design.

**INTRODUCTION**

Ligand-induced activation of receptor tyrosine kinases such as the epidermal growth factor receptor (EGFR) promote the subsequent activation of downstream signaling pathways, which in turn drive pro-proliferative and survival cellular signals.¹ In a subset of non-small cell lung cancer (NSCLC) patients, EGFR has gained activating mutations such as L858R and exon 19 deletion, which largely renders the receptor constitutively activated, independent of ligand stimulation.² This results in sustained hyper-activation of signaling pathways downstream of EGFR, such as AKT (protein kinase B) and ERK (extracellular signal-regulated kinase), and promotes the oncogenic dependency of the cell on these pro-proliferative and survival drives resulting from the mutated EGFR. Therefore, inhibition of activated EGFR using small-molecule kinase inhibitors prevents its signaling and reduces the oncogenic drive, ultimately resulting in the inhibition of tumor growth.

First generation EGFR tyrosine kinase inhibitors (TKIs) such as gefitinib and erlotinib are now established therapies in NSCLC patients having activating mutations in EGFR.^{3,4} Around 70% of patients respond initially but develop resistance with a median time to progression of 10–16 months. In at least

50% of these initially responsive patients, disease progression is associated with the gain of a secondary mutation, T790M in exon 20 of EGFR (typically referred to as the gatekeeper mutation), in combination with an activating mutation.⁵

The specific mechanism by which the activating mutants exert their effect is not entirely clear, but studies on the L858R mutation have shown there to be a decreased affinity for ATP (Figure 1).⁶ It has been proposed that the activating mutations may favor the active conformation of the kinase to which compounds such as gefitinib (1)⁴ and erlotinib (2)⁷ may bind (Figure 2).⁸ Further reports have suggested additional and alternative mechanisms of activation, including the differential ability of the mutants to sample the active and inactive conformations.^{9,10} However, the secondary mutation, T790M, increases the affinity of the kinase for ATP.^{6,11} An increase in the kinase domain's ATP affinity reduces the inhibitory activity of ATP-competitive inhibitors such as gefitinib and erlotinib against EGFR. This amino acid is known as the gatekeeper residue, and it is positioned at the entrance of what is typically

Received: June 3, 2013

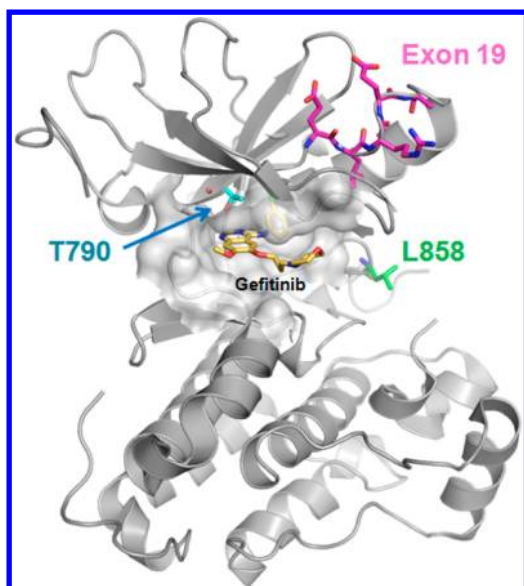


Figure 1. Location of activating (L858R and exon 19 deletion) and resistant secondary mutations (T790M) in the kinase domain of EGFR (PDB code 2ITY¹³).

referred to as the back pocket.¹² The size and nature of this residue has a significant effect on determining which

compounds are tolerated in this region of the binding site. It is therefore also possible that there is a steric component to the resistance mechanism against early EGFR inhibitors, which specifically affects compounds such as gefitinib and erlotinib that were identified by targeting the wild-type threonine gatekeeper. In addition, it has been proposed that the T790M mutation can lead to differential structural rearrangements of the protein across inhibitor classes,⁹ impacting the potency and selectivity of compounds against the mutations.

A number of second-generation irreversible inhibitors were subsequently developed on the basis of the anilinoquinazoline template of gefitinib. These inhibitors contained an acrylamide functionality that covalently targets Cys-797, which is positioned in the solvent channel of the kinase.^{14,15} Such reported compounds include afatinib, **3**,¹⁶ canertinib, **4**,¹⁷ and dacomitinib, **5**,¹⁸ shown in Figure 2. The covalent mechanism is thought to overcome the increase in ATP affinity of the double mutant, resulting in the potent activity of these compounds in cellular models. However, Cys-797 is present in all relevant forms of EGFR; these second-generation compounds, therefore, not only have increased activity against the activating and resistant mutations but also against wild-type EGFR. The inhibition of wild-type EGFR is not thought to contribute to their clinical efficacy but is thought to be responsible for the side-effects of skin rash and diarrhea.¹⁹ As these side effects are

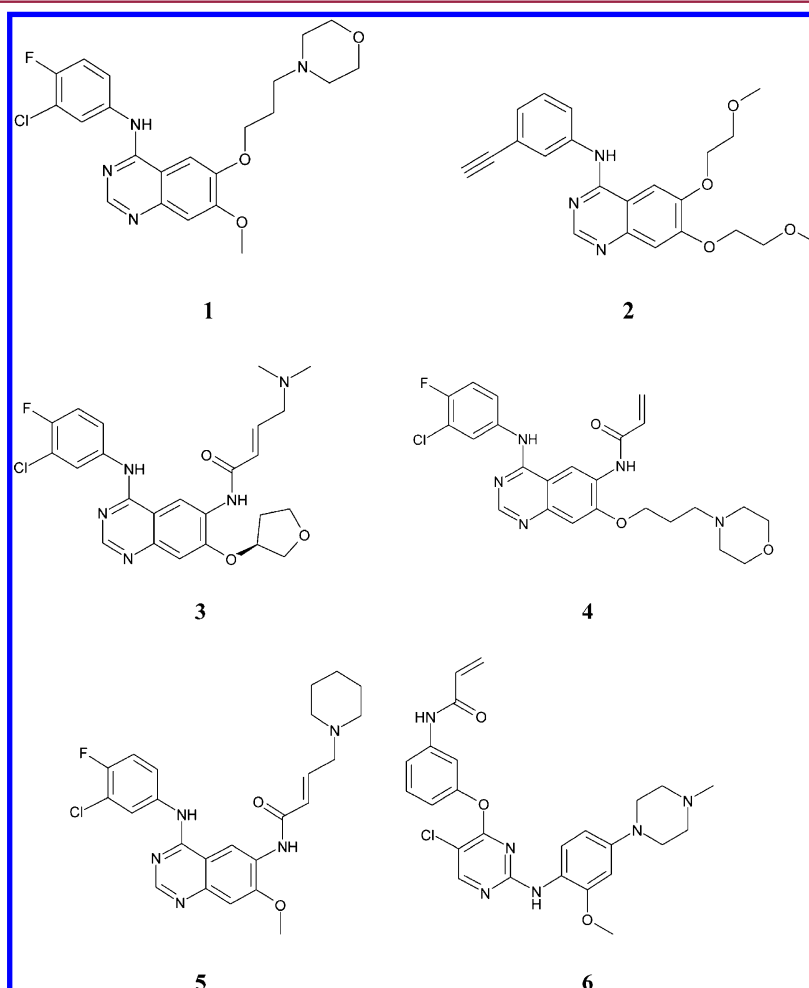
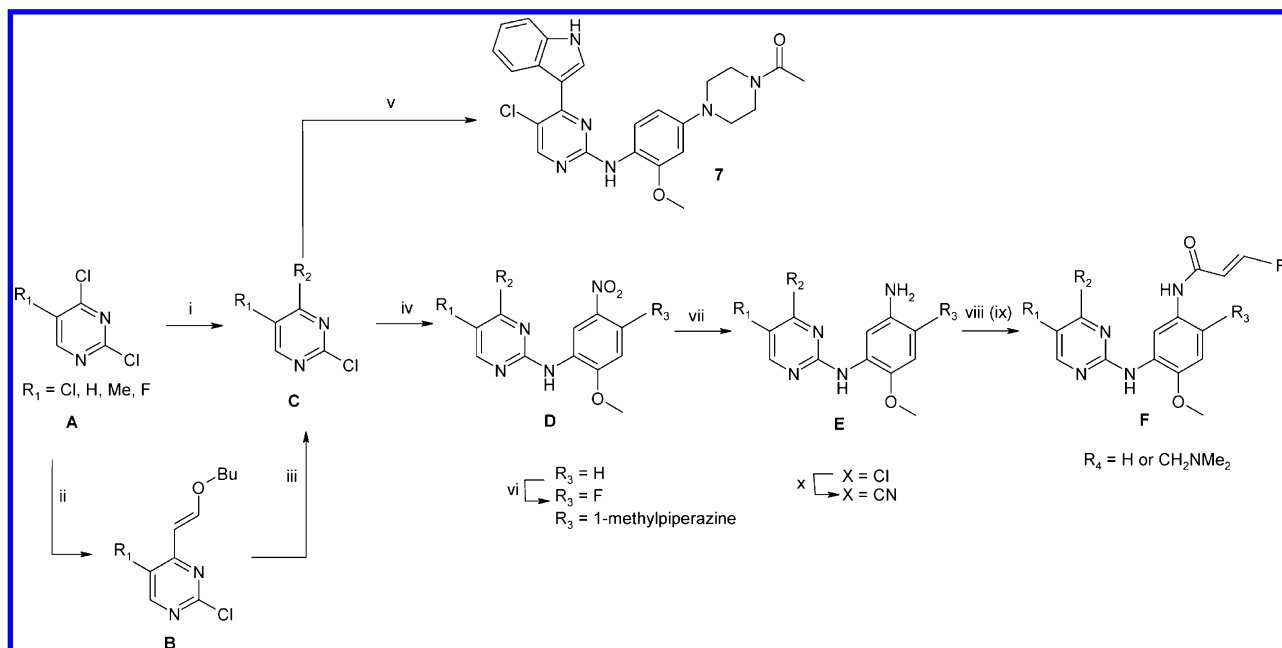


Figure 2. Selection of published EGFR inhibitors disclosed in the literature.

Scheme 1. General Synthesis Approach to the Key Novel Compounds (Table 1) Reported in This Manuscript^a

^aReagents and conditions: (i) Aniline displacement: excess NaHCO₃, 2-pentanol or EtOH, 85 °C; Suzuki coupling: Na₂CO₃, ArB(OR)₂, Pd(PPh₃)₄, MeCN, water, 100 °C; indole displacement: MeMgBr (1 equiv, 3.2 M in 2-methyl THF), indole (1 equiv), THF, 0–60 °C. (ii) Et₃N (1.1 equiv), butyl-vinyl-ether (1.1 equiv), Pd(OAc)₂ (0.03 equiv), PEG 200, 80 °C. (iii) Either 1-aminopyridinium iodide (1 equiv), K₂CO₃ (2.5 equiv), DMA, 110 °C or 2-amino-pyridine (1 equiv), NBS (1.2 equiv), 1,4-dioxane, water, 85 °C. (iv) Either aniline (1.1 equiv), *p*-TSA (1.1 equiv), 2-pentanol, 80–120 °C, or aniline (1.1 equiv), 4 M HCl in 1,4-dioxane, TFE, 150 °C (*μ*W), or aniline (1.1 equiv), Pd(OAc)₂ (0.08 equiv), Xantphos (0.1 equiv), Cs₂CO₃ (2 equiv), 1,4-dioxane, 80 °C. (v) Acetyl aniline (1 equiv), *p*-TSA (3 equiv), *n*-pentanol/NMP, 150 °C. (vi) 1-Methylpiperazine (2.5 equiv), TFE, 120 °C. (vii) Either aniline (3 equiv), NH₄Cl (0.7 equiv), EtOH, water, 100 °C or Pt/C (1 equiv), ZnI₂ (0.1 equiv), H₂, MeOH, EtOAc. (viii) Either acryloyl chloride (1M, THF, 1 equiv), DIPEA (1.1 equiv), THF, 0 °C, or (*E*)-4-(dimethylamino)but-2-enoic acid (1 equiv), HATU (1.1 equiv), DIPEA (2.5 equiv), DCM, or (*E*)-4-bromobut-2-enoic acid (1.1 equiv), HATU (1.1 equiv), DIPEA (2.5 equiv), 0 °C then Me₂NH (20 equiv). (ix) Deprotection (where required): Either K₂CO₃ (3 equiv), THF, MeOH or Cs₂CO₃ (3 equiv), THF, MeOH, 0 °C. (x) Zn(CN)₂ (0.6 equiv), Zn (0.1 equiv), Pd₂(dba)₃ (0.1 equiv), dicyclohexyl(2',4',6'-triisopropylbiphenyl-2-yl)phosphine (0.2 equiv), DMA, 90 °C.

typically dose limiting in patients, it is possible that the activity of these inhibitors against wild-type EGFR will limit their achievable activity against the T790M mutation in patients.

Our initial aim was to identify a double-mutant-selective template by exploiting the differences in the properties of the respective threonine and methionine gatekeeper residues. We hypothesized that exploiting the methionine gatekeeper residue to leverage the increased potency might lead to a selectivity profile in which the compounds are active against the double mutant enzyme but with reduced activity against wild-type EGFR. Ideally, compounds would also show greater activity against the activating EGFR mutations than against wild-type EGFR.

From the time that we initiated our efforts to identify compounds with this preferred selectivity profile, other compounds have been reported that exploit similar principles. An early published example was from the Dana-Farber Cancer Institute (WZ-4002, **6**)²⁰ and was based on a pyrimidine template. More recently, additional covalent inhibitors from Clovis Oncology (CO-1686) and Hanmi Pharmaceuticals (HM61713) are reported to be in clinical studies, although their chemical structures are yet to be disclosed. Also reported is the reversible anaplastic lymphoma kinase (ALK) inhibitor (AP26113) from ARIAD, with reported activity against the double mutant form of EGFR. Further publications have also been disclosed, from the time that we initiated this work, reporting on other potential compound series active against the EGFR double mutation.^{21–23}

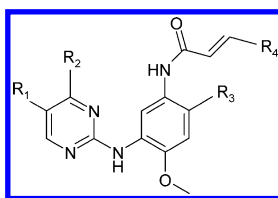
RESULTS AND DISCUSSION

Chemistry. Where possible, compounds were prepared according to the general strategy outlined in Scheme 1 from commercially available pyrimidines (**A**). Installation of the reactive warhead, where present, at the last or penultimate step was desirable because it was not expected to be robust enough during further chemical manipulation. Although Scheme 1 captures the synthesis approach to the majority of the key examples from this manuscript (shown in Table 1), because of the structural diversity of the compounds reported, some examples were not synthesized using this approach. However, the full synthesis of all compounds can be found in the Experimental Section or in the Supporting Information.

Installation of the 4-substituent of the pyrimidine was achieved by direct regioselective displacement of 4-chloro under basic conditions or by Suzuki coupling. Where necessary, the aryl group was constructed from vinyl butyl ether intermediate **B**, which in turn was synthesized from the 4-chloro-pyrimidine via Heck coupling. Subsequent cyclization reactions afforded aryl pyrimidines **C**.

The aniline addition to 2-chloropyrimidines **C** was achieved via Buchwald–Hartwig coupling with substituted anilines or by acid-catalyzed S_NAr reaction, typically by heating with *p*-TSA in 2-pentanol. For compounds where R₃ = H, commercial 5-nitro-2-methoxy-aniline was used. Where R₃ = F, the aniline was not commercially available and was synthesized by nitration of 2-methoxy-4-fluoro-aniline prior to use. Amine substitution of the fluorine by S_NAr proceeded in fair to good yield by heating with either an excess of the amine or using DIPEA as base.

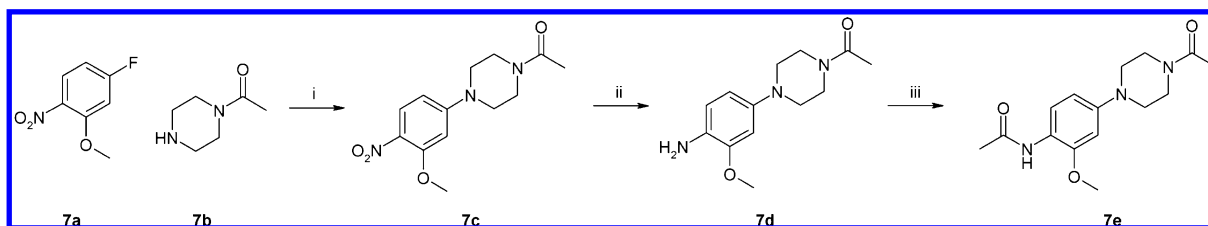
Table 1. Novel Compounds from This Manuscript Synthesized Using Scheme 1



Compound	R ₁	R ₂	R ₃	R ₄
9	Cl		H	H
15	Cl		H	CH ₂ NMe ₂
16	H		H	CH ₂ NMe ₂
17	F		H	CH ₂ NMe ₂
18	Me		H	CH ₂ NMe ₂
37	Cl		H	H
39	Cl		H	CH ₂ NMe ₂
40	CN		H	CH ₂ NMe ₂
42	Cl		H	H
45	Cl		H	CH ₂ NMe ₂
56	Cl			H
57	H			H
58	Cl			H
59	H			H

Subsequent reduction of the nitro group and reaction with acryloyl chloride ($R_4 = H$) or HATU coupling with commercial (*E*)-4-(dimethylamino)but-2-enoic acid yielded test compounds F in moderate yield.

For compound 7, which does not contain an acrylamide, the anilino substituent could be installed fully elaborated. This portion was constructed from commercial starting materials, as detailed in Scheme 2.

Scheme 2. Synthesis of the Intermediate for Compound 7^a

^aReagents and conditions: (i) 1-Acetyl piperazine (1.2 equiv), DIPEA (1 equiv), DMA, 90 °C, 18 h, 90%. (ii) Platinum oxide (5 mol %), EtOH, hydrogen (1.3 bar), 3 h, 99%. (iii) Acetic anhydride (6.6 equiv), acetic acid (4.5 equiv), 1 h, 73%.

The full synthesis and characterization of the novel compounds within this manuscript is detailed in the Experimental Section (key compounds 7, 9, 15, and 58) and in the Supporting Information for the remaining examples.

Activity Profile of Published EGFR Inhibitors. We measured the cellular activity of a number of known inhibitors against the different forms of EGFR (Table 2) using phosphorylation

Table 2. Cellular Activity Profile of Published EGFR Inhibitors against the Double Mutant (DM), Activating Mutant (AM), and Wild-Type (WT) Enzymes^a

compound	DM cell (μM)	AM cell (μM)	WT cell (μM)	DM/WT margin
Gefitinib (1)	3.3	0.0087	0.062	0.02
Erlotinib (2)	7.6	0.0059	0.077	0.01
Afatinib (3)	0.023	0.00057	0.012	0.53
Dacomitinib (5)	0.042	0.00063	0.011	0.27
WZ-4002 (6)	0.023	0.044	1.18	51

^aActivity data in this manuscript are quoted as the geometric mean IC_{50} of at least three independent measurements. The DM/WT margin is calculated by dividing the mean wild-type IC_{50} by the mean double-mutant IC_{50} .

end points. These included the wild-type enzyme (WT) with a human LoVo cell line and the exon 19 deletion activating mutation (AM) using a PC9 cell line. Activity against the L858R/T790M double-mutant enzyme (DM) was measured using a NCI-H1975 cell line. Although much of this data set was already in the public domain from a number of different groups, it was useful to measure their activities in consistent assays to allow an accurate comparison of their profile across the mutants.

As expected, gefitinib and erlotinib were shown to be active against wild-type EGFR and to have a greater activity against the activating mutant but significantly reduced cellular activity against double-mutant EGFR (3.3 and 7.6 μM , respectively). Afatinib (3) and dacomitinib (5) have increased activity against wild-type and activating-mutant EGFR along with increased activity against the double mutant compared to gefitinib and erlotinib. However, the potency of these compounds against the double mutant is lower than the potency against wild-type EGFR (i.e., double mutant to wild-type margin of <1). WZ-4002 (6) is more active against the double-mutant enzyme and maintains activity against the activating mutant but with a margin over the wild-type enzyme broadly consistent with the published data.²⁴

Identification of Double-Mutant-Selective Templates.

To identify mutant-selective templates, a set of compounds was selected and tested against the EGFR wild-type and double-mutant enzymes using biochemical assays at an external CRO²⁵ (Figure 3). This compound set included some reversible EGFR inhibitors from our compound collection (red) along with a

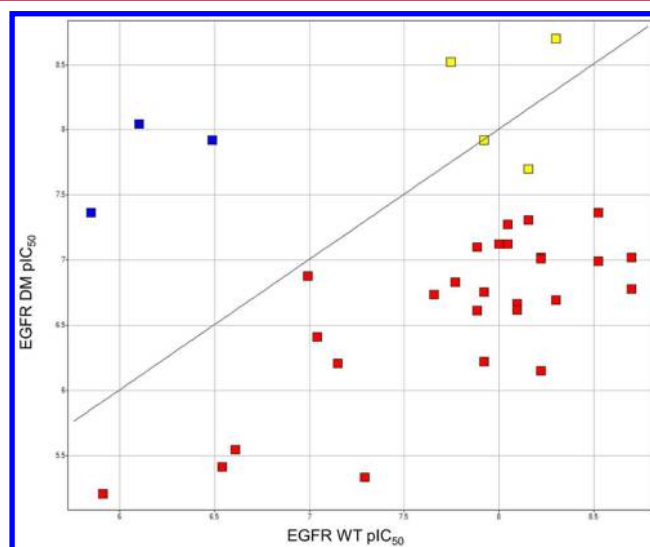
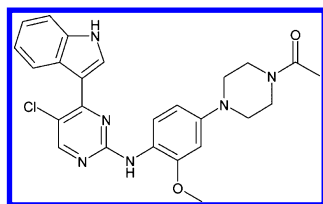


Figure 3. EGFR wild-type (WT) and T790M/L858R (DM) biochemical inhibition data on a probe set of compounds. Red points show reversible EGFR inhibitors, yellow points show covalent EGFR inhibitors, and blue points show selected compounds from internal AstraZeneca projects. Compound activity is expressed as a pIC_{50} .

selection of published irreversible EGFR inhibitors (yellow) for reference. Additional examples of compounds from our collection were added that have shown activity against kinases with methionine gatekeepers during previous AstraZeneca drug-discovery projects (blue). The reversible EGFR inhibitors showed increased activity against the wild-type enzyme when compared to the double mutant, consistent with the described activity profiles of gefitinib and erlotinib. The irreversible anilinoquinazoline-based EGFR inhibitors (including 3, 4, and 5) showed significant activity in both assays, consistent with an increase in activity from the formation of the covalent bond. Note that it is difficult to accurately compare the relative potencies of the reversible versus irreversible compounds in these assays because of their different mechanism of action, with irreversible inhibitors often demonstrating time-dependent inhibition.^{26,27} However, the set of compounds that was of particular interest were the examples from internal AstraZeneca projects that had shown activity against kinases with a methionine gatekeeper.

Interestingly, these compounds were active against double-mutant EGFR with selectivity over wild-type, a common feature of which was a pyrimidine core. A representative example, 7 (Table 3), contains an indole headgroup with an IC_{50} of 0.009 μM against the double mutant and with an 88-fold selectivity over wild-type EGFR. Although this reversible inhibitor was active in this biochemical double-mutant assay, we observed a large

Table 3. Identified Double-Mutant (DM)-Selective Reversible EGFR Inhibitor

compound	DM enzyme (μM)	WT enzyme (μM)	DM/WT selectivity	DM cell (μM)
7	0.009	0.79	88	0.77

enzyme-to-cell drop-off of around 90-fold when it was tested in our double-mutant cellular assay (IC_{50} 0.77 μM), which is likely driven by the high ATP affinity of this enzyme and the high ATP concentration present in the cellular environment.²⁸ Therefore, we aimed to convert compound 7 into a covalent inhibitor to partially overcome the effect of the increased affinity of ATP for the mutant kinase while hoping to maintain the intrinsic selectivity over the wild-type enzyme.

Structure-Based Design Targeting Cys-797. A predicted binding mode of compound 7 was modeled using GLIDE,²⁹ utilizing a public domain crystal structure of the EGFR-T790M mutation (PDB code 2JIT⁶) following protocols detailed in the Supporting Information. Although this structure does not contain an activating mutation, we hoped that it would be adequate for the modeling of potential binding modes that we could exploit by structure-based design.

Of the various potential binding modes suggested by the modeling, we decided to progress with the hypothesis that the pyrimidine core of the molecule formed a hydrogen bond to the kinase hinge, specifically to the backbone of Met-793 (Figure 4). In this binding mode, the chlorine substituent is

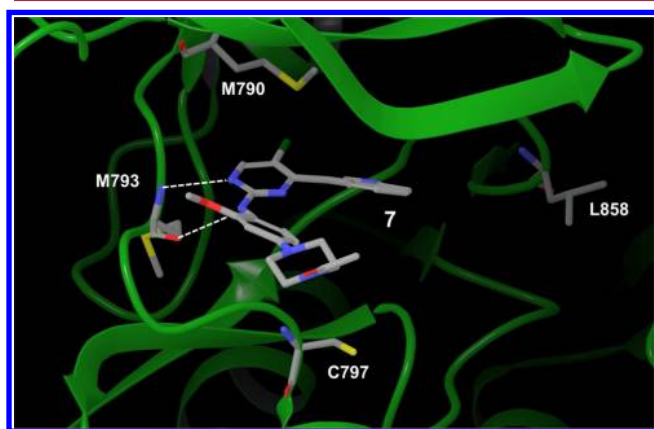


Figure 4. Modeled binding mode of compound 7 in a published EGFR crystal structure (PDB code 2JIT) that contains a T790M mutation.

directed toward the methionine gatekeeper. The indole group is positioned adjacent to the region of the kinase referred to as the back pocket. The anilino group of the inhibitor is oriented toward the solvent channel of the ATP pocket and was predicted to form an additional hydrogen bond to the hinge. Assuming this modeled binding mode, we attempted to design compounds with a reactive substituent positioned in a manner that would enable targeting Cys-797 via the formation of a

covalent bond. The meta position of the aniline appeared to be the most suitable location, and such examples were prioritized. A range of different substituents were modeled to estimate their potential to target Cys-797, and from this work we decided to incorporate an acrylamide-based side chain. A particular example of interest was compound 8, which showed improved cellular activity in the activating- and double-mutant cell assays with selectivity over wild-type (Table 4).

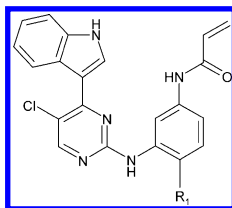
From a set of further analogues synthesized, an example with an ortho-methoxy group at R₁ (compound 9) showed increased biochemical and cellular activity. Further examples were synthesized with the acrylamide attached to different regions of the molecule. Interestingly, moving the acrylamide to the para position (compound 10), which is also likely to be positioned near Cys-797, appears not to result in covalent inhibition (Table 5). Compound 10 showed only moderate activity in the double-mutant biochemical assay (0.3 μM) and minimal activity in cellular assays. The acrylamide was also appended to a dihydroindole ring; however, this compound (11) was less potent in the double-mutant assays (0.052 and 2.1 μM vs enzyme and cell, respectively). Furthermore, nitrile-based compound 12 was synthesized in an attempt to form a reversible covalent interaction resulting in a thioimidate adduct, as preceded in cysteine and serine protease inhibitors.³⁰ Although this compound was active in the double-mutant biochemical assay (IC_{50} 0.065 μM), 12 showed minimal cellular activity (IC_{50} 2.8 μM), suggesting that this functional group was perhaps not suitable for the cysteine in EGFR or that a suitable geometry had not been achieved for the covalent bond to form.

To gain further confidence that our early compounds would be able to form the desired covalent bond, 9 was prioritized for crystallization in an EGFR wild-type structural system, which was available via an external CRO.³¹ The binding mode of compound 9 was subsequently solved (PDB code 4L15), as shown in Figure 5, demonstrating that a covalent bond was formed to Cys-797. In this case, the binding mode of this template in the EGFR receptor was consistent with the binding mode found in our earlier modeling work.

Focus on Reducing Lipophilicity. One of the key issues with our initial compounds described above was their high lipophilicity ($\text{LogD}_{7.4} > 4.3$). This level of lipophilicity can often translate into poor physicochemical properties and pharmacokinetics (PK), hindering later development.^{32,33} We were also keen to ensure low activity against the hERG potassium ion channel. A key aim of the evolution of this series was therefore to reduce the overall lipophilicity, indicated in subsequent tables by the experimental $\text{LogD}_{7.4}$ measurements, while retaining the existing levels of EGFR potency and the favorable selectivity profile. The activity and wild-type selectivity of subsequent compounds was monitored using in-house cellular assays. We no longer routinely measured the biochemical activity of our compounds.

To improve the physical properties of compounds within this series, we decided to modify what we referred to as the head group. In addition, we decided to assess the effect of the addition of a basic group to the acrylamide (Table 6). Out of these head groups, the pyrrolopyridine system (compound 13) was especially interesting, maintaining reasonable potency in our double- and activating-mutant cell assays (IC_{50} 0.033 and 0.15 μM) but with an improved margin to wild-type EGFR (390-fold). Furthermore, the basic acrylamide-based side chains of template B (examples 14 and 15), although showing a small decrease in activity of 2 to 3 fold compared to the neutral

Table 4. Activity Data for Synthesized Inhibitors Targeting Cys-797 Using the Acrylamide Functionality



compound	R ₁	DM enzyme (μM)	AM cell (μM)	DM cell (μM)	WT cell (μM)	DM/WT selectivity	LogD _{7.4}
8	H	0.053	0.27	0.081	3.5	43	>4.3
9	OMe	0.0063	0.029	0.022	0.55	25	>4.3

Table 5. Activity Data for Synthesized Compounds Exploring SAR around the Covalent Bond Interaction



Compound	R ₁	DM Enzyme (μM)	AM Cell (μM)	DM Cell (μM)	WT Cell (μM)	DM/WT Selectivity
10		0.32	19	12.9	>30	>1.6
11		0.052	2.8	2.1	>30	>15
12		0.065	1.8	2.8	>30	>11

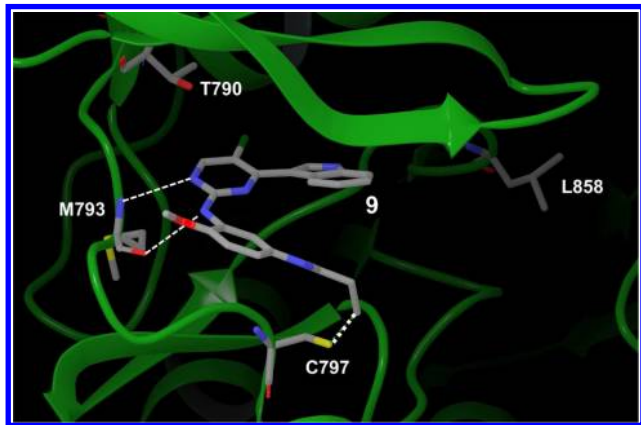
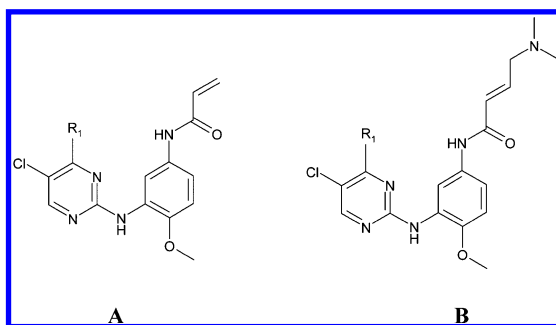


Figure 5. Protein crystal structure of compound 9 bound in wild-type EGFR. The described covalent bond to Cys-797 is shown (PDB code 4LI5).

equivalents, did show a marked reduction in LogD_{7.4} to a level at which meaningful experimental values could be measured. On the basis of the overall potency, selectivity, and physical property profile of 15, this compound was selected as a key in vivo probe compound for this template. These compounds also began to populate a more favorable area of physicochemical property space, with a LLE (ligand lipophilicity efficiency) of 3.4 for example 15 using the double-mutant cell assay and experimental LogD_{7.4}.

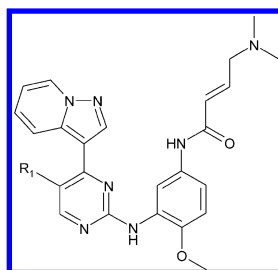
Investigating the Effect on 5-Position Substituents on the Pyrimidine. The 5-position of our template was predicted by our modeling to be positioned adjacent to the gatekeeper residue, so we thought that varying this position may have some interesting effects on the potency and selectivity of compounds within our series. Our initial hit contained chlorine in this position, which is relatively lipophilic; therefore, varying this group offered the potential for compound lipophilicity to be

Table 6. Activity and Lipophilicity Data for Compounds Targeting an Improved Physicochemical Property Space



Compound	Template	R ₁	AM Cell (μM)	DM Cell (μM)	WT Cell (μM)	DM/WT Selectivity	LogD _{7.4}	LLE ^a (DM)
9	A		0.029	0.022	0.55	25	>4.3	<3.4
13	A		0.15	0.033	12.8	390	>4.3	<3.2
14	B		0.085	0.053	1.55	29	4.1	3.2
15	B		0.40	0.096	23	240	3.6	3.4

$${}^a\text{LLE (DM)} = \text{pIC}_{50} \text{ DM (cell)} - \text{LogD}_{7.4}$$

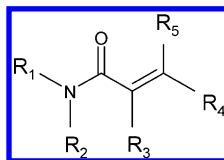
Table 7. Activity and Lipophilicity Data of Compounds Exploring the Effect of the 5-Substituent Position (R₁) on the Pyrimidine

compound	R ₁	AM cell (μM)	DM cell (μM)	WT cell (μM)	DM/WT selectivity	LogD _{7.4}	LLE (DM)
15	Cl	0.40	0.096	23	237	3.6	3.4
16	H	0.39	0.25	20	80	2.6	4
17	F	0.38	0.22	19	85	3.3	3.4
18	Me	0.25	0.29	24	82	3	3.5
19	S(=O)Me	1.3	15.2	>30	>2	1.3	3.5

reduced.³⁴ A range of 5-substituted compounds was subsequently prepared and assessed across our in-house cellular assays (Table 7).

The range of R₁ substituents that we investigated varied in both size and lipophilicity. Although potency varied across the

double-mutant cell assay, the LLE (using the double-mutant cell data) remained constant at around 3.4 to 3.5 except for R₁=H where it was increased to 4. This was an interesting result because removing the chlorine of compound 15 (giving compound 16) reduced LogD_{7.4} by an order of magnitude

Table 8. Glutathione (GSH) Reactivity of 6-Membered Ring Aromatic Model Compounds^a

compound	GSH $t_{1/2}$ (min)	Log k_{GSH}^* ($\text{M}^{-1} \text{s}^{-1}$)	R_1	R_2	R_3	R_4	R_5	$R_1 \sigma_{\text{meta}}$	$R_1 \sigma_1$
20	816	-2.51	4-aminophenyl	H	H	H	H	-0.006	0.052
21	323	-2.11	4-fluorophenyl	H	H	H	H	0.12	0.13
22	2940	-3.07	benzyl	H	H	H	H	-0.08	0
23	436	-2.24	phenyl	C	H	H	H	0.06	0.12
24	299	-2.08	phenyl	H	H	H	H	0.06	0.12
25	428	-2.23	2-methylphenyl	H	H	H	H	0.07	0.119
26	524	-2.32	4-methoxyphenyl	H	H	H	H	0.05	0.11
27	37.2	-1.17	2-cyanophenyl	H	H	H	H	0.18	0.194
28	145	-1.76	3-fluorophenyl	H	H	H	H	0.15	0.16
29	361	-2.16	4-methylphenyl	H	H	H	H	0.06	0.1
30	22	-0.94	2-pyridyl	H	H	H	H	0.33	0.25
31	32.9	-1.12	4-cyanophenyl	H	H	H	H	0.221	0.175
32	>8640	< -3.54	tert-butyl-phenyl	H	C	H	H	-0.043	0.05
33	>10 000	< -3.60	phenyl	H	C	H	H	0.06	0.12
34	>10 000	< -3.60	phenyl	H	H	C	C	0.06	0.12
35	>10 000	< -3.60	phenyl	H	H	C	H	0.06	0.12

^aThe full list of the explicit structures for compounds in this table can be found in Table S1 of the Supporting Information. Note that the rate constant, k , was derived using [GSH] 4.61 mM. σ values were determined using ACD/Laboratories software (version 12.01). All compounds with an absolute rate constant showed a more polar product peak of mass parent +307 except for example 22 where no products were observed (reflecting a much slower reaction compared to other compounds coupled to the detection limits of LC-MS).

(3.6 compared to 2.6) and might allow the physicochemical properties of this series to be improved further. Although the double-mutant activity was reduced for compound 16, compared to 15 (0.25 vs 0.096 μM) the activity against the activating-mutant form was unchanged (0.39 vs 0.40 μM). The double-mutant selectivity of 16 was reduced to 80-fold, from 237-fold, for compound 15, potentially resulting from chlorine interacting more effectively with the methionine gatekeeper residue. However, our collective data on these compounds suggested that it might be possible to achieve reasonable potency in the EGFR double and activating mutants while leveraging the selectivity over wild-type without a chlorine in the 5-position. We postulated that removing the chlorine might improve the physicochemical properties via the reduction in overall lipophilicity of these molecules.

Modulating Compound Reactivity. The potency of covalent inhibitors is influenced by both the reversible binding properties of the compound to the protein (K_i) and the ability of the compounds to covalently bind to a suitable residue in the active site (k_{inact}). As such, it is important to aim for compounds of sufficient chemical reactivity toward an active-site residue (in this example cysteine) while balancing against unwanted off-target binding that could lead to high compound clearance and/or idiosyncratic toxicity.³⁵ One method of optimizing covalent compounds in this way is through the measurement of the k_{inact}/K_i values for compounds within a series. This approach, however, proved technically challenging using our assays, so we were unable to exploit it for driving SAR routinely.²⁶ Our alternative approach was to establish a suitable 'reactivity window' for our compounds and to develop an understanding of how to synthesize compounds that were more likely to fall within the intended range. As a measure of thiol reactivity, we have used an assay based on determining the second-order rate constant (k_{GSH}) for the reaction of our compounds with glutathione (GSH).³⁶⁻³⁸

To determine the structural and electronic features that influenced the chemical reactivity of our compounds, a set of six-membered aromatic ring acrylamide-containing models were initially investigated in the glutathione assay (Table 8). These model acrylamides have relatively good aqueous solubility and thus we avoid any complication of reaction kinetics that might have arisen because of precipitation issues. All compounds investigated were stable in phosphate buffer alone at pH 7.4. In the presence of glutathione, a simple addition reaction (Scheme 3) was observed, generating the more polar glutathione adduct, which is seen by liquid chromatography-mass spectrometry (LC-MS) as a mass increase of 307 units.

The Hammett plots in Figure 6 enable a quantitative understanding of the relationship between the electronic effects exerted through the R_1 position of the acrylamide, expressed as σ values, and glutathione reactivity. Consequently, this knowledge can be applied to design elaborated compounds that sit in the desired reactivity window using appropriate $R_1 \sigma$ values. From our results set, the rate of the reaction appeared to be dependent on the electron-withdrawing ability of groups in the R_1 position (Figure 6) of the acrylamide. In particular, the inductive effect of the R_1 group (represented either as σ_{meta} or σ_{ind}) was seen to determine thiol reactivity with ρ values of 5.56 and 9.23, respectively. The addition of further electronic descriptors such as σ_{para} or σ_{meso} to the Hammett equations (1) and (2) in Figure 6 did not appear to be significant. Such inductive electron withdrawal at the R_1 position would be consistent with enhanced polarization of the alkene bond via carbonyl conjugation and also serves to stabilize the enolic transition state. The introduction of methyl groups onto either the α or β carbon of the model acrylamides (R_3 and R_4) resulted in no reaction being observed with glutathione, ruling out these substituents as options on elaborated compounds. A similar decrease in thiol reactivity following methylation at

Scheme 3. Addition Reaction of Model Compounds with Glutathione

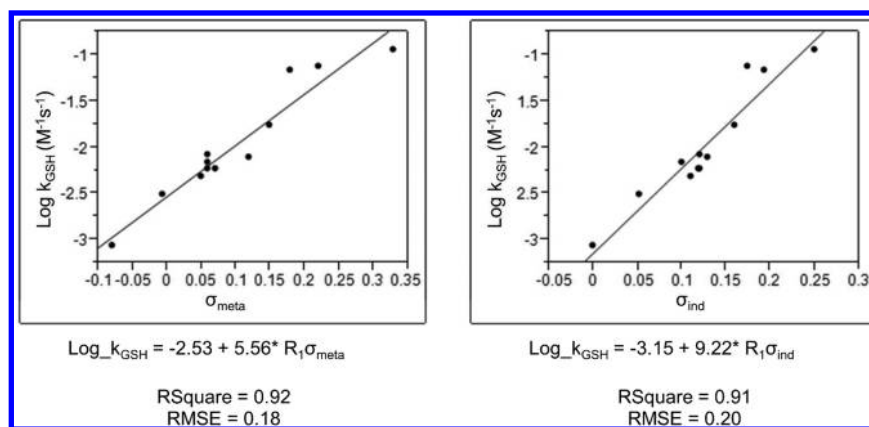
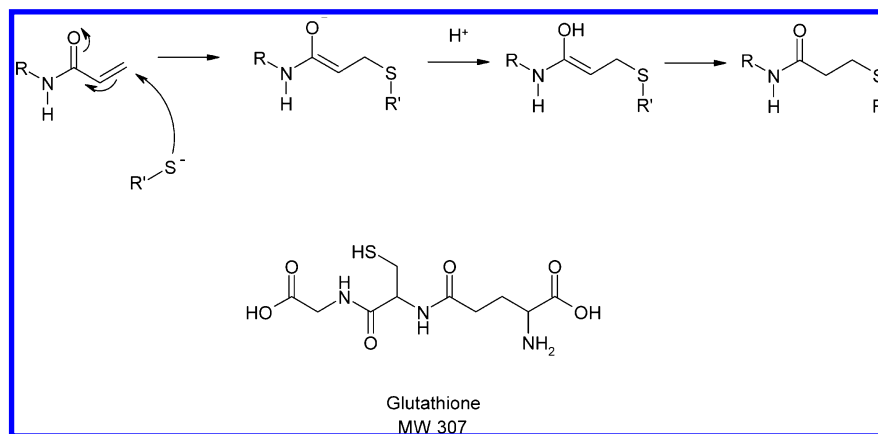


Figure 6. Hammett plot of σ_{meta} and σ_{ind} properties versus compound reactivity ($\text{Log } k_{\text{GSH}}$) across the model compound set.

the α and β carbon has been observed by other workers in their investigations with α,β -unsaturated aldehydes, ketones, esters, acids, and amides.^{39–42} Engels et al. calculated via quantum mechanical/molecular modeling (QM/MM) an increased energy barrier to methyl thiolate attack on α,β -unsaturated phenyl ketones with an elevated energy of the enolate intermediate upon methylation at the α and β positions, suggesting steric effects as a possible reason for such a reactivity change.⁴¹ Although other workers have similarly suggested steric effects as an explanation for decreased reactivity for α and β methylation,³⁹ Kerske et al. argue that reactant stabilization by hyperconjugation of α and β methyls and not steric hindrance is the reason for the lowered reactivity.⁴²

Table 9 captures the glutathione reactivity constant data of more elaborated compounds. This compound set consists of examples containing pyrimidine, anilinoquinazoline, and anilinoquinoline scaffolds. To increase the diversity of the structures within this data set, we have also included examples from an additional template we identified on the basis of a bis-anilino-pyrimidine scaffold, some examples from which have since been disclosed in the literature.⁴³

With the more diverse elaborated compounds (Figure 7), the dependence of reactivity on the inductive effect at R_1 as expressed by $R_1 \sigma_{\text{meta}}$ is observed across a variety of R_1 templates and fits the same Hammett line as seen with the model systems. This suggests that the learning from our model systems can be applied to more leadlike molecules.

Looking across the anilino-pyrimidine-containing compounds (core i, Table 9), there is a consistent drop in reactivity of

0.43 in $\text{Log } k_{\text{GSH}}$ (factor 2.7) on substituting hydrogen for methoxy in the R_4' position of the aniline (matched pairs 36/14 and 43/44). In contrast, varying the substituent at R_5' (cyano, methyl, hydrogen, and chlorine) on the pyrimidine had no significant effect on reaction rate, with the largest difference in $\text{Log } k_{\text{GSH}}$ being 0.13 (factor 1.3). This is consistent with the increased distance of R_5' from the acrylamide group, thereby exerting minimal electronic effect. Similarly, varying the R_4' position in the quinoline series (core iv, examples 53 and 54) produced no significant effect on the reaction rate. There are, however, clear outliers on the Hammett plot in Figure 7. Compound 46 shows a significantly faster reaction than was expected from an R_1 inductive effect alone. Analysis of the reaction products of 46 using LC–MS indicates the substitution of the morpholine group for glutathione (Scheme 4). The increased reaction rate is believed to be due to intramolecular base catalysis by the α -morpholine group, which is able to form a six-membered hydrogen-bond ring in the transition state, facilitating nucleophilic attack. Two mechanisms can be postulated to occur, namely, a two step addition/elimination with the morpholine stabilizing the enolate transition state (Scheme 4a) or a concerted reaction where the morpholine base activates the glutathione by removal of a proton (Scheme 4b). Identifying which of these mechanisms is dominant is not clear on the basis of the present data. In work by Tsou et al. that looked at quinazoline acrylamides, the activation of glutathione by α -morpholine has been proposed as a mechanism to explain the observed reactivity in a competition assay in THF/ H_2O /Methanol.⁴⁴

Compound **41** (core ii) also appeared to react more quickly than expected from the σ_{meta} value. The reason for this is unclear, but the reaction represents the only example in this data set involving a five-membered heterocyclic substituent attached to the acrylamide. Also of interest was **38**, which proved to be highly unstable in pH 7.4 buffer alone. The introduction of the dimethylaminobenzyl group into the acrylamide phenyl ring facilitated rapid intramolecular attack by the amine to form a stable cyclic quaternary ion (Scheme 5 and Figure S1, Supporting Information).

Substitution at the acrylamide α and β positions, R_1' and R_2' , with a cyclic piperidine (**47** and **48**, Figure 8) resulted in no measurable reaction with glutathione. This indicates that the electronic activation afforded by the electron-withdrawing partially protonated amine groups (pK_a of 7.9 and 7.4, respectively) toward the α and β carbons is insufficient to overcome the steric barrier from the ring.

Interestingly, other workers have shown that the introduction of electron-withdrawing groups cyano and hydroxyl at the α and β positions of alkenals and acrylates affords an enhanced reaction rate with thiols.^{39,45} When the dimethyl amine group is introduced as a pendant substituent at the β -carbon in **15** (pK_a 7.8), a measurable reaction with glutathione is observed (Table 8). Unfortunately, the matched pair compound of **15** without the pendant amine group was too insoluble to measure a

glutathione reaction constant, but the matched pair of **44** and **45** reveals that the pendant amine group does not offer a significant enhancement of the reaction rate over the unsubstituted compound (factor of 2). This is borne out by Figure 7, where compounds with (+) and without (open squares) a pendant base (β substituent R_1') both sit on the same Hammett equation line. Significantly enhanced reactivity resulting from the pendant base (+) would have been seen as points sitting above the line. Because an electronically significant difference would not be expected in terms of the amine-group activation of the β carbon between **15** and **48**, this suggests that the unconstrained pendant base in **15** offers less steric resistance to glutathione attack than **48**. The unconstrained β -pendant base in **15** would also be expected to more readily be able to undertake intramolecular base catalysis than **48**, but no significantly enhanced reaction rate is observed. This contrasts with earlier studies by Tsou et al. who showed a significant enhancement when a β -pendant base was added to quinazoline acrylamides in a competition assay.⁴⁴ It is suggested that this difference may be due to solvent effects.

Alternative thiol reactive groups to acrylamides, namely, acetylenes and ethene sulphonamides have also been investigated in the glutathione assay (**49**, **50**, **51**, and **52**, shown in Table 10).

Table 9. Glutathione (GSH) Reactivity Data of Elaborated Acrylamide-Containing Compounds^a

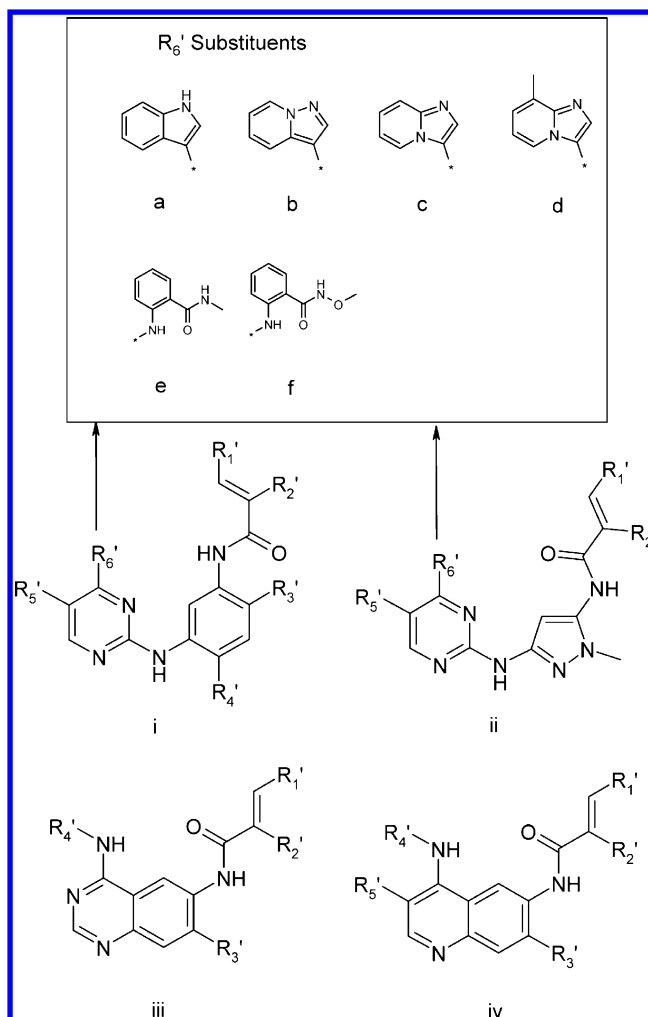


Table 9. continued

ID	GSH $t_{1/2}$ (min)	Log k_{GSH} ($M^{-1}s^{-1}$)	$R_1 \sigma_{meta}$	R_1'	R_2'	R_3'	R_4'	R_5'	R_6'	Core
3	25	-1	0.34	N,N-dimethylaminomethyl	H		3-Cl, 4-F phenyl	-	-	iii
4	23	-0.96	0.33	H	H		3-Cl, 4-F phenyl	-	-	iii
5	49.3	-1.29	0.31	piperidin-1-ylmethyl	H	methoxy	3-Cl, 4-F phenyl	-	-	iii
14	442	-2.25	0.07	N,N-dimethylaminomethyl	H	H	methoxy	Cl	a	i
15	352	-2.15	0.07	N,N-dimethylaminomethyl	H	H	methoxy	Cl	b	i
16	440	-2.24	0.07	N,N-dimethylaminomethyl	H	H	methoxy	H	b	i
18	479	-2.28	0.07	N,N-dimethylaminomethyl	H	H	methoxy	Me	b	i
36	173	-1.84	0.091	N,N-dimethylaminomethyl	H	H	H	Cl	a	i
37	364	-2.16	0.07	H	H	H	methoxy	Cl	c	i
38	<66	>-1.42	0.08	H	H	N,N-dimethylaminomethyl	methoxy	Cl	c	i
39	298	-2.08	0.07	N,N-dimethylaminomethyl	H	H	methoxy	Cl	d	i
40	413	-2.22	0.07	N,N-dimethylaminomethyl	H	H	methoxy	cyano	b	i
41	32	-1.11	0.1	H	H	-	-	Cl	b	ii
42	1231	-2.69	0.07	H	H	H	methoxy	Cl	f	i
43	328	-2.12	0.092	H	H	H	H	Cl	e	i
44	924	-2.57	0.07	H	H	H	methoxy	Cl	e	i
45	453	-2.26	0.07	N,N-dimethylaminomethyl	H	H	methoxy	Cl	e	i
46	16.8	-0.83	0.07	H	methyl-morpholine	H	methoxy	Cl	e	i
47	>2000	<-2.9	0.07			H	methoxy	Cl	b	i
48	>2000	<-2.9	0.07			H	methoxy	Cl	b	i
53	31	-1.09	0.33	N,N-dimethylaminomethyl	H	ethoxy	3-Cl, 4-F phenyl	cyano	-	iv
54	41	-1.21	0.33	N,N-dimethylaminomethyl	H	ethoxy		cyano	-	iv
55	76.9	-1.49	0.22	H	H	H	2-methylphenyl	-	-	iii

^aThe full list of the explicit structures for compounds in this table can be found in Table S2 of the Supporting Information. * $R_1 \sigma_{meta}$ is defined in the scheme in Table 8 and all other substituents are defined in the figure above.

Comparing the matched pairs **44/51** and **42/52** indicates that both acetylenes and ethene sulphonamide groups are significantly more reactive to glutathione than acrylamides (26.4 and 26.9 times more reactive, respectively). Interestingly, when a pendant dimethyl amine base is added to the acetylene group in **49**, the compound is >58.7 times more reactive than the acrylamide matched pair **15**, suggesting that the basic group has a significant activating effect not observed with acrylamides. This is also supported by a comparison of **49** with **51**, which both share the same $R_1 \sigma_{meta}/\sigma_I$ values but show >5.8 fold difference in glutathione reactivity when the pendant base is added to the acetylene. **52** also shares the same σ_{meta}/σ_I values as **49** and **51**, indicating that the ethene sulphonamide group

has comparable glutathione reactivity to the acetylene group (cf. **51**). As with the acrylamides, the substitution of a methyl group at the β position of the acetylene (**50**) deactivates the acetylene to thiol reaction. Comparing compound **50** to acrylamide **55**, which share the same $R_1 \sigma_{meta}/\sigma_I$ values (differing in their R_1 structure by a distal Br for Me change on aniline R_3 substituent), shows that the methyl acetylene is 2.6 times less reactive to glutathione than the acrylamide.

A selection of compounds from both the model and elaborated series covering a range of reactivities with glutathione were also studied in the presence of the human glutathione-S-transferase enzyme (Supporting Information,

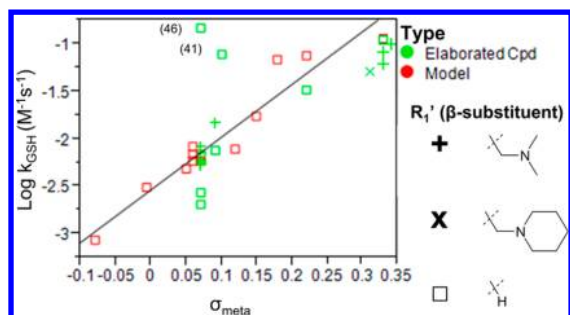


Figure 7. Reactivity data for elaborated acrylamide compounds overlaid onto $\text{Log } k_{\text{GSH}}$ versus σ_{meta} Hammett plot for model systems. Data on the model-system compounds (Table 8) are shown in red and elaborated compounds (Table 9) are shown in green. The data is further classified by a selection of the β substituents (R_1') defined in Table 9 (not defined for compounds 47 and 48 because of a lack of observed reactivity).

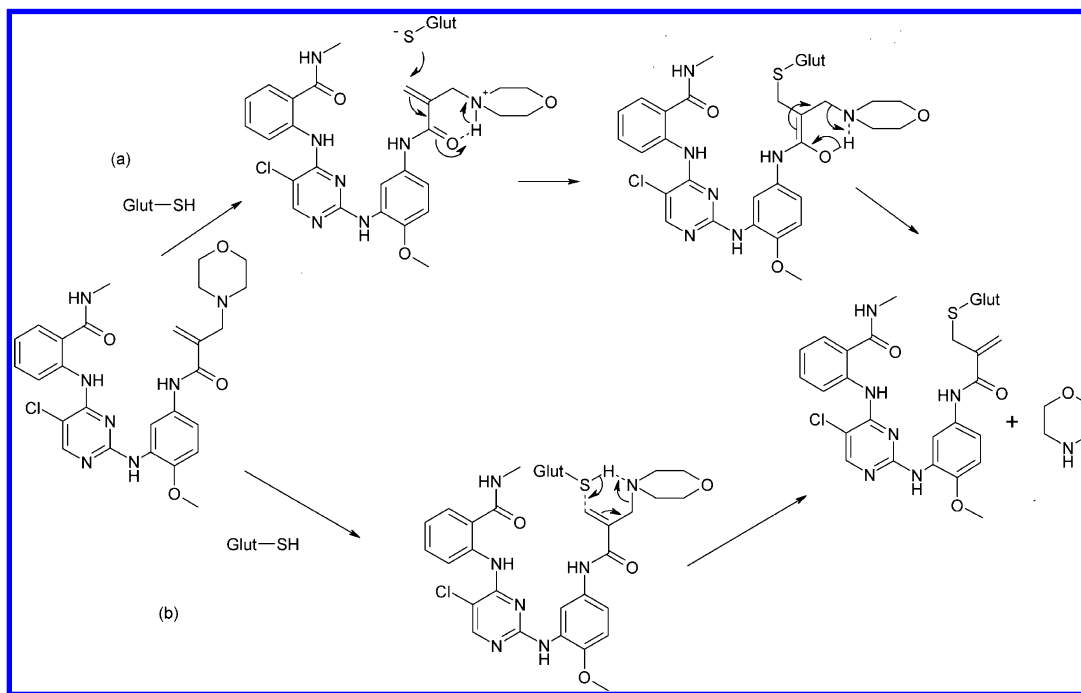
Table S3). This revealed that the glutathione reaction was not catalyzed by the glutathione-S-transferase enzyme.

In seeking to define a suitable 'reactivity window', the elaborated compounds studied for glutathione reactivity were simultaneously analyzed in the double-mutant cell assay. Figure 9 reveals the relationship between the target potency and

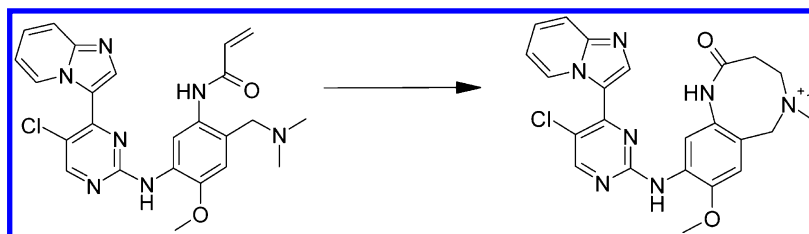
glutathione reactivity for the data set discussed in this section. As we hoped, there is not a strong correlation because the initial target noncovalent binding (K_i) will play a key part in defining potency (R^2 0.52 and RMS 0.53). The noncovalent contribution to the binding is essential for driving the selectivity of these compounds over other proteins with accessible cysteine residues. However, there is a general trend toward more reactive compounds showing increased activity, and compounds with pIC_{50} values >7 for the most part tend to have glutathione half-lives <400 min. As such, we took a glutathione half-life of 400 min as a guide for a suitable lower limit of reactivity. Afatinib (3) is currently in phase III clinical studies, and the reported clinical side effects of the compound appear to be linked to the inhibition of wild-type EGFR rather than off-target effects resulting from covalent binding. As such, this seemed to be a good compound to benchmark in our glutathione assay, generating a half-life of 25 min. Therefore, we used a half-life of 25 min as the higher limit to the window of reactivity that we aimed to work within.

Further Optimizing of the Lead Series. Our aim was to increase further the potency of our series by exploiting additional interactions with the protein along with the learning from our exploration of compound reactivity. As part of this, we synthesized a set of compounds with a piperazine substituent on the para position of the aniline (Table 11). We expected

Scheme 4. Postulated Mechanisms for the Nucleophilic Substitution Reaction Observed for Compound 46 with Glutathione



Scheme 5. Proposed Intramolecular Reaction of Compound 38 in Buffer at pH 7.4^a



^aFormation of cyclic quaternary confirmed by MSMS $m/z = 478.18$.

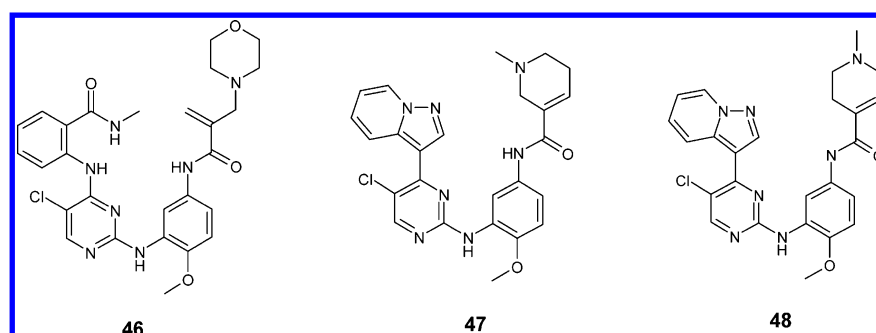


Figure 8. Novel compounds reported in this manuscript containing alpha substitutions (R_2').

Table 10. Selection of Alternative Covalent Modifying Groups to Acrylamide Synthesized as Part of This Work^a

ID	Structure	GSH $t_{1/2}$ (min)	Log k_{GSH} ($M^{-1}s^{-1}$)	$R_1 \sigma_{meta}$	$R_1 \sigma_{ind}$
49		<6	>-0.38	0.07	0.133
50		199	-1.9	0.22	0.219
51		35.4	-1.15	0.07	0.132
52		46	-1.26	0.07	0.132

^aThe R_1 substituent is defined in Table 8.

that the addition of the piperazine adjacent to the acrylamide would effect the conformation and geometry of both substituents, so we were keen to assess whether this combination was compatible with good potency on our template. We combined this change with the 5-position SAR described in the previous section using both our indole and pyrrolo-pyridine head groups.

The data on this compound set suggests a general improvement in potency with the addition of the piperazine substituent. Compound **56** is more potent than **15** in both primary cell assays (0.14 vs 0.4 μM in the activating-mutant and 0.019 vs 0.096 μM in the double-mutant assays), maintaining a good selectivity for the double mutant over wild-type of 620-fold. There is also a small increase in reactivity with glutathione for compound **56** ($t_{1/2}$ 188 min) compared to 352 min for com-

pound **15**, which is consistent with the small increase in electron-withdrawing ability of the group attached to the acrylamide nitrogen (σ_{meta} 0.09 compared to σ_{meta} 0.07). A number of factors could influence this increase in activity, including the preference for a basic group in this region of the protein, the increased compound reactivity, and the effect on acrylamide geometry. The LLE of these compounds is generally improved, with **56** showing an increased LLE of 4.1 compared to 3.4 for **15**. Removal of the chlorine (compound **57**) showed a reduction in double-mutant cellular activity, 0.071 μM compared to 0.019 μM , but no effect on activating-mutant activity, as observed previously. The transferring of this learning back to the indole head group identified compounds that were significantly more potent against the activating and double mutant. Example **58** is a particularly potent compound, with an LLE of 4.6.

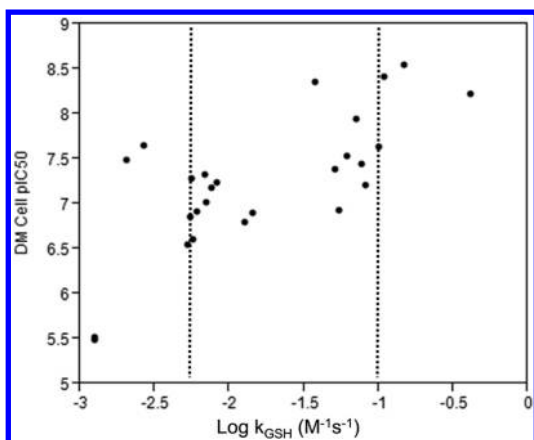
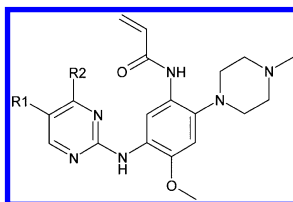


Figure 9. Compound reactivity measured by $\text{Log } k_{\text{GSH}} (\text{M}^{-1} \text{s}^{-1})$ plotted against EGFR double-mutant (DM) cellular pIC_{50} for the elaborated compounds reported in this manuscript. Dashed lines indicate the 'reactivity window' in which the design of novel compounds was subsequently focused.

The data on these compounds is also consistent with the early data on this head group, with the indole-containing compounds showing a reduced margin with wild-type EGFR (140-fold and 19-fold for **58** and **59**, respectively), albeit with greater absolute double-mutant activity. Whether a more potent EGFR double- and activating-mutant inhibitor with a smaller margin to wild-type is preferable over a less potent inhibitor with a greater margin to wild-type will require further assessment.

In Vivo Efficacy of Compound 15. Compound **15** was identified as a suitable in vivo proof-of-concept compound from our scoping work. To build further confidence in the covalent mechanism of action, the equivalent nonreactive propionamide was synthesized (compound **60**, Figure S2, Supporting Information), showing a lower double-mutant biochemical activity ($0.018 \mu\text{M}$) and significantly reduced cellular activity ($2.3 \mu\text{M}$). Although not the most potent (or wild-type selective) example synthesized, the overall balance of properties identified **15** as having an acceptable combination of activity and pharmacokinetic (PK) properties to validate our approach (Table 12). In addition, **15** demonstrated encouraging antiproliferative activity when tested in our H1975 (double mutant), PC9 (activating mutant), and Calu3 (wild-type) cell lines with an EC_{50} of 0.099, 0.14, and $1.78 \mu\text{M}$ respectively. This profile is consistent with our described cellular data showing significant activity in the double and activating mutants with selectivity over the wild-type enzyme. Subsequently, **15** was orally dosed in an in vivo efficacy study using an H1975 double-mutant xenograft model in immune-compromised mice (Figure 10). Briefly, tumor cells were inoculated subcutaneously, and the mice were randomized into groups of 4–10 mice prior to compound dosing when tumors reached approximately $0.2\text{--}0.4 \text{ cm}^3$. Tumor growth was measured from the start of treatment, assessed by comparison of the mean change in the tumor volume for the control and treated groups, and represented as tumor growth inhibition (where $>100\%$ TGI is a regression from the starting size). Statistical significance was evaluated using a one-tailed t test. Compound **15** showed significant efficacy of 105% total growth inhibition (TGI) after 7

Table 11. Activity and Lipophilicity Data on Compounds with the Addition of a Piperazine Group



Compound	R ₁	R ₂	AM Cell (μM)	DM Cell (μM)	WT Cell (μM)	DM/WT Selectivity	LogD _{7.4}	LLE(DM)
56	Cl		0.14	0.019	12	620	4.1	4.1
57	H		0.14	0.071	19	270	NT	-
58	Cl		0.023	0.0056	0.77	140	3.7	4.6
59	H		0.017	0.068	1.3	19	3.4	3.7

Table 12. Overview of Activity, Physicochemical, and PK Data of Compound 15

compound	AM cell (μM)	DM cell (μM)	WT cell (μM)	solubility (μM) ^a	PPB (% free) (M/R/H) ^b	Human Heps Clint ($\mu\text{L min}^{-1} \times 10^6$ cells)	Rat Heps Clint ($\mu\text{L min}^{-1} \times 10^6$ cells)	hERG (μM)	Rat PK CL/F ^c
15	0.40	0.096	23	1.6	1.2/1.2/0.8	<3	18	4.2	8.1/45%

^aSolubility was evaluated under thermodynamic conditions using crystalline solid. ^bPlasma protein binding (PPB) was assessed by equilibrium dialysis in the appropriate species (mouse/rat/human) at 37 °C. Free and bound concentrations were quantified by LC-MS. ^cIntravenous clearance ($\text{mL min}^{-1} \text{kg}^{-1}$) was assessed in male Han Wistar rats when dosed with a 3 $\mu\text{mol kg}^{-1}$ solution. Oral bioavailability was observed with a 6 $\mu\text{mol kg}^{-1}$ solution dosed in male Han Wistar Rats.

Table 13. Summary of the Efficacy Data from Xenograft Studies on Compound 15 Compared to Gefitinib (1)^b

compound	oral dose (mg/kg/day)	H1975 (% TGI)	PC9 (% TGI)	A431 (% TGI)
15	60	105 ($p < 0.001$)	134 ($p < 0.01$)	46 ($p < 0.05$)
Gefitinib (1)	6.25	8 ($p \text{ NS}$) ^a	142 ($p < 0.001$)	79 ($p < 0.001$)

^aData from a 100 mg/kg/day oral dose of gefitinib. ^bStatistical significance (p values in brackets) was calculated from compound-treated and vehicle groups using a one-tailed t -test. NS indicates that the % TGI was not significant compared to the vehicle-treated group.

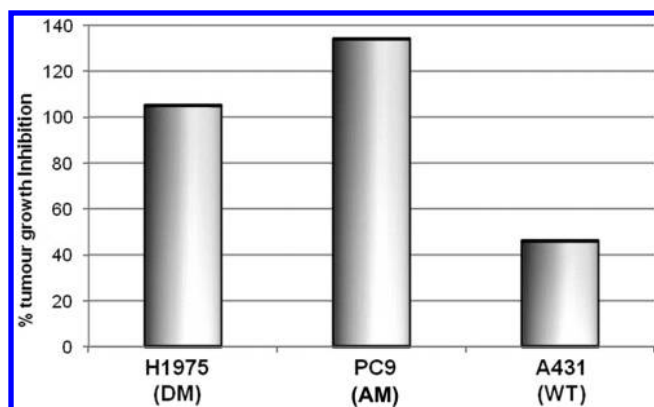


Figure 10. Antitumor efficacy study data on compound 15 across the double (H1975), activating (PC9), and wild-type (A431) EGFR xenograft models. Tumor growth inhibition (% TGI) was calculated between the compound treated and vehicle groups, with a % TGI > 100 indicating tumor regression from the initial tumor size.

days at an oral dose of 60 mg/kg/day (formulated as the mesylate salt). This dose and formulation was chosen because we had observed good exposure in the nude (C_{max} of 7.1 μM and AUC_{0-t} 48.2 $\mu\text{M h}$) and severe-combined immunodeficiency (SCID) (C_{max} 8.1 μM and AUC_{0-t} 119.3 $\mu\text{M h}$) mice that are used in these models, which also compared well with the rat PK reported in Table 12 (C_{max} of 5.32 μM and AUC_{0-t} 92.7 $\mu\text{M h}$).

Compound 15 was subsequently taken into an efficacy study in a PC9 activating-mutant cell line and a wild-type A431 cell line in immunocompromised mice. The activity against the PC9 xenograft model at the same dose (134% TGI, resulting in tumor regression) was also encouraging, and the compound showed reduced activity against the A431 xenograft model (46% TGI), as was hoped from the wild-type margin demonstrated from the in vitro cellular profile.

As a comparison, an oral dose of gefitinib of 6.25 mg/kg/day (representative of the clinically relevant human dose), showed 142% TGI in the PC9 xenograft model and 79% TGI in the A431 xenograft model after 7 days (Table 13). Gefitinib showed little activity in the H1975 xenograft model, even at the higher oral dose of 100 mg/kg/day, which resulted in an 8% TGI (not significant) after 7 days.

Kinase Selectivity of Compound 15. Compound 15 was submitted to a broad panel of >70 diverse kinases at The University of Dundee,⁴⁶ where it was tested at a concentration of 1 μM in biochemical assays to assess wider kinase selectivity.

The compound showed >75% inhibition for 10 kinases, which were IGF1R, insulin receptor (IR), CAMKKbeta, CHK2, PBK, FLT1, MAP3K11, smMLCK, BTK, and MELK. However, out of these kinases, only BTK has a cysteine in the same position as EGFR, so the mode of inhibition is likely to be via a reversible mechanism toward the majority of these targets. The full selectivity profile of compound 15 can be viewed in the Supporting Information (Table S4). We do not believe these off-target activities contributed to the efficacy in the reported xenograft models; however, information on the optimization of the selectivity profile of this series will be reported in future disclosures.

CONCLUSIONS

We have reported the development of a series of potent inhibitors of the activating and resistant mutants of EGFR with varying degrees of selectivity over the wild-type enzyme. This activity profile across the mutants would appear to be suitable to demonstrate activity against the activating and resistant mutants of EGFR but with an improved margin to toxicity associated with wild-type activity. As part of this approach, we simultaneously optimized the covalent and noncovalent elements of binding into a suitable range to identify compounds with satisfactory potency and intrinsic reactivity. This approach may be exploited more generally to optimize covalent inhibitors across a broader range of targets. Also reported is encouraging antitumor efficacy in H1975 double-mutant and PC9 activating-mutant models with compound 15. This compound was also observed to have significantly lower activity in the A431 model used here as a measure of EGFR wild-type activity. However, the relatively poor solubility (1.6 μM) and the hERG IC_{50} of 4.2 μM demonstrated the need for further development efforts for this compound and across the scaffold more generally. Further evolution of this series will be reported at a later date; in particular, this will focus on improving the potency, kinase selectivity, and properties of the series toward a clinical candidate.

EXPERIMENTAL SECTION

Biochemical and Cellular Activity Assays. Compounds were tested at a range of concentrations. The mean data values for each concentration along with untreated control wells and 100% inhibition/competition control wells were used to derive a plot of inhibition/competition against concentration. Origin software was used to interpolate the IC_{50} values by nonlinear regression.

Kinase Inhibition Assay Using HTRF (Homogenous Time-Resolved Fluorescence). The inhibitory activity of compound against the kinases EGFR (T790M/L858R) was determined with

CisBio HTRF (homogenous time-resolved fluorescence) KinEASE TK (#62TKOPEC). The enzyme reaction contains recombinant N-terminal GST-tagged human EGFR (T790M/L858R), which phosphorylates the HTRF tyrosine kinase biotinylated substrate. The sequence of the substrate is proprietary to CisBio. Compounds were serially diluted in 100% (v/v) DMSO before being acoustically dispensed from an Echo 555 (Labcyte) into black Corning 1536-well assay plates. Kinase activity assays were performed in a total reaction volume of 3 μ L per well. A 1.5 μ L enzyme reaction consisted of 1.6 nM EGFR (T790M, L858R), 1 mM DTT, and 10 mM MgCl₂. A 1.5 μ L substrate mix consisted of 1 μ M TK substrate, 30 μ M ATP, 1 mM DTT, and 10 mM MgCl₂. Following a 50 min incubation, 3 μ L of stop mix was added, which consisted of 250 nM Strep-XL665 and TK Ab-Cryptate diluted in kit detection buffer. The plates were incubated for 1 h before being read on Pherastar using standard HTRF settings. N-terminal GST-tagged recombinant human EGF receptor, with amino acids 696-end containing the T790M and L858R mutations, was obtained from Millipore.

Measurement of Cellular Phosphorylation Assay. For EGFR (T790M/L858R), the human lung cell line NCI-H1975 was obtained from the American Type Culture Collection. For EGFR (Exon 19 deletion), the human lung cell line PC9 was obtained from the Akiko Hiraide from Preclinical Sciences R&D AZ Japan. The growth media was RPMI 1640 containing 10% fetal calf serum and 2 mM glutamine. For EGFR (wild type), the human colon adenocarcinoma cell line LoVo was obtained from the European Collection of Cell Cultures. LoVo growth media was RPMI 1640 containing 3% charcoal-stripped fetal calf serum and 2 mM glutamine. All cells were used from assay-ready frozen cryo banks. Assays to measure cellular phosphorylation of endogenous p-EGFR in cell lysates were carried out according to the protocol described in the R&D Systems DuoSet IC Human Phospho-EGFR ELISA (R&D Systems, no. DYC1095). Following thawing and resuspension, 40 μ L of cells were seeded (10 000 cells/well for NCI-H1975 and PC9 or 15 000 cells/well for LoVo) in growth medium in Corning black, clear-bottomed 384-well plates and incubated at 37 °C with 5% CO₂ overnight. The cells were acoustically dosed using an Echo 555 with compounds serially diluted in 100% DMSO (v/v). The cells were incubated for a further 2 h and following aspiration of medium, 40 μ L of 1 \times lysis buffer was added to each well. LoVo were stimulated with EGF (25 ng/mL) for 10 min before lysis. Greiner black high-bind 384-well plates were coated with capture antibody and then blocked with 3% BSA. Following the removal of the blocking solution, 15 μ L of lysate was transferred to the Greiner black high-bind 384-well plates and incubated for 2 h. Following aspiration and washing of the plates with PBS/A, 20 μ L of detection antibody was added and incubated for 2 h. Following aspiration and washing of the plates with PBS/T, 20 μ L of QuantaBlu fluorogenic peroxidase substrate (Thermo-Fisher Scientific, no. 15169) was added and incubated for 1 h. Twenty microliters of QuantaBlu stop solution was added to the plates, and fluorescence was read on an Envision plate reader using an excitation wavelength of 352 nm and an emission wavelength of 460 nm.

Experimental Procedure for Cellular Proliferation Experiments. Cell lines were plated in 384-well plates at between 500 and 1000 cells per well, depending on the cell line, in 70 μ L per well of RPMI media containing 10% fetal calf serum, 2 mM L-glutamine, and 1% penicillin/streptomycin. The cells were allowed to attach overnight at 37 °C under 5% CO₂. The following day, titrations of test compound were added to the assay plates using an Echo Liquid Handler Labcyte, and the treated cells were incubated for a further 72 h at 37 °C under 5% CO₂. Each compound was tested as an 11-point dose response, with a top concentration of 10 μ M using 1:3 dilutions. Following a 72 h incubation of the compound-treated plates, 5 μ L of 2 μ M SYTOX Green Nucleic Acid Stain, Life Technologies was added per well, and the plates were incubated at room temperature for 1 h. The number of fluorescent cells per well was measured with an Acumen TTP LabTech Ltd., with this number representing the dead cell count. Ten microliters of 0.25% saponin was added per well, and the plates were incubated overnight at room temperature. The total number of fluorescent cells per well was acquired with the Acumen. The number of dead cells was subtracted

from the total number of cells, and the live cell number was plotted to determine EC₅₀ values.

X-ray Crystallography. The kinase domain of the wild-type EGFR protein was expressed in Sf9 insect cells as a GST-fusion protein with a thrombin cleavage site.⁴⁷ After affinity purification and cleavage of the GST tag, a gel-filtration step was performed, and the resulting protein was concentrated to 6 mg/mL. Apo crystals were prepared using the vapor-diffusion technique by drops equilibrated against 0.2 M NH₄Cl and 1.2 M Na-K-tartrate buffered with 10 mM acetate at pH 4.6 and 0.15 M hepes, pH 7.0. Protein–ligand complex crystals were generated by soaking apo-crystals with 2 mM of the compound (dissolved in DMSO at 100 mM). The Free Mounting System (Proteros biostructures³¹) was used for cryo cooling. Diffraction data were collected at the Swiss Light Source at 100 K on a Pilatus6M detector, and the data was processed using XDS and XSCALE.⁴⁸ The crystallographic model was completed in Coot⁴⁹ and refined with Refmac5.⁵⁰ Crystallographic data and refinement parameters are summarized in Table 14.

Table 14. Crystallographic Data Collection and Refinement Summary

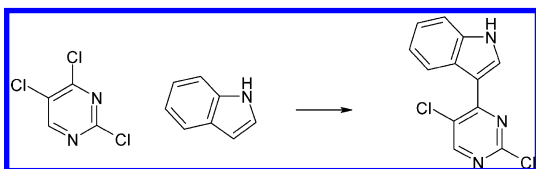
data collection statistics	
Cell: a = b = c, $\alpha = \beta = \gamma$ (Å, deg)	144.89, 90
resolution (Å)	2.64 (2.96–2.78) ^a
unique reflections	15 026 (2185) ^a
multiplicity	24.4 (25.5) ^a
completeness (%)	99.9 (100.0) ^a
R _{sym} (%)	9.2 (44.5) ^a
mean (I)/sd	32.02 (9.75) ^a
refinement statistics	
number of reflections (working/test)	14 487/539
R/R _{free} (%)	16.5/20.3
number of atoms	
protein	2245
water	69
ligand	30
ions	1
deviation from ideal geometry	
bond lengths (Å)	0.007
bond angles (deg)	1.04
bonded B's (Å ²)	2.10
Ramachandran plot	
most favored region	92.1
additional allowed region	7.9
generously allowed region	0
disallowed region	0

^aData in parentheses refer to the highest resolution shell.

Synthesis and Characterization of Key Compounds 7, 9, 15, and 58. General Chemistry Statement. Microwave reactions were performed using one of the following reactors: Biotage Initiator, Personal Chemistry Emrys Optimizer, Personal Chemistry Smithcreator, or CEM Explorer. Work-up procedures were carried out using traditional phase-separating techniques or by using strong cation-exchange (SCX) chromatography using an Isolute SPE flash SCX-2 column (International Sorbent Technology Limited); when necessary, organic solutions were dried over anhydrous MgSO₄ or Na₂SO₄. Flash column chromatography (FCC) was performed on Merck Kieselgel silica (Art. 9385), on Silicycle cartridges (40–63 μ m silica, 4–330 g weight), or on Grace resolv cartridges (4–120 g) either manually or automated using an Isco Combi Flash Companion system. Preparative reverse-phase HPLC (RP HPLC) was performed with C18 reversed-phase silica, for example, with a Waters Xterra or XBridge preparative reversed-phase column (5 μ m silica, 19 mm diameter, 100 mm length) or with a Phenomenex Gemini axia preparative reversed-phase column (5 μ m silica, 110A, 21.1 mm diameter, 100 mm length) using decreasingly polar mixtures as eluent (e.g., 1–5% formic acid or 1–5%

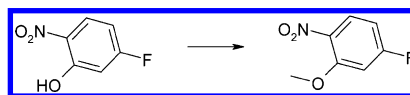
aqueous ammonium hydroxide ($d = 0.88$) as solvent A and acetonitrile as solvent B or MeOH/MeCN 3:1. The intermediates were not necessarily fully purified, but their structures and purity were assessed by TLC, NMR, HPLC, and mass spectral techniques, and they are consistent with the proposed structures. The purities of compounds used for biological testing were assessed by NMR, HPLC, and mass spectral techniques, and they are consistent with the proposed structures; the purity was $\geq 95\%$. FT ^1H and ^{13}C NMR spectra were obtained either with a 400 MHz (^1H , 400 MHz; ^{13}C , 101 MHz), 500 MHz (^1H , 500 MHz; ^{13}C , 126 MHz), or 700 MHz (^1H , 700 MHz; ^{13}C , 176 MHz) Bruker spectrometer. ^1H and ^{13}C shifts are given in ppm and are measured relative to the internal residual solvent peak (CDCl_3 , 7.25 ppm/77 ppm). Peak multiplicities are expressed as follows: s, singlet; d, doublet; dd, doublet of doublets; t, triplet; br s, broad singlet; and m, multiplet. Analytical HPLC was performed on C18 reverse-phase silica with a Phenomenex Gemini reversed-phase column (5 μm silica, 110 A, 2 mm diameter, 50 mm length) using decreasingly polar mixtures as eluent (e.g., decreasingly polar mixtures of water containing 0.1% formic acid or 0.1% ammonia as solvent A and acetonitrile as solvent B or MeOH/MeCN 3:1), with a flow rate of about 1 mL/min. Detection was by electrospray mass spectrometry and by UV absorbance at a wavelength of 254 nm. Electrospray mass spectral data were obtained using a Waters ZMD or Waters ZQ LC/mass spectrometer acquiring both positive and negative ion data, and generally, only ions relating to the parent structure are reported. Accurate mass and MSMS fragmentation data were obtained using a ThermoScientific hybrid LTQ-FT mass spectrometer with an Agilent 1100 quaternary pump with PDA and Autosampler. Five microliters of sample dissolved in 50:50 acetonitrile/water in 0.1% formic acid was injected onto a Thermo Scientific Hypersil Gold 50 \times 2.1 mm, 5 μm particle LC column. The gradient was 5–100% B over 17 min, with a 3 min re-equilibration time at 5% B. The flow rate was 0.5 mL/min, with A being 0.1% formic acid in water and B being 0.1% formic acid in acetonitrile. The MS and MSMS spectra were obtained in ESI +ve mode in both the ion trap and ion cyclotron resonance (ICR) cell using helium as the collision gas at a normalized collision energy of 35 eV. The ICR cell was run at resolution settings of 25 000 in MS mode and 12 500 in MSMS mode.

Synthesis of Compound 7. 3-(2,5-Dichloropyrimidin-4-yl)-1H-indole (61).

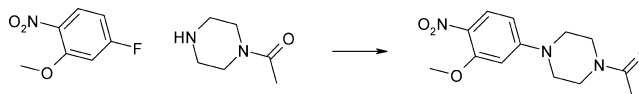


Methylmagnesium bromide (3.2 M in 2-methyltetrahydrofuran, 3.37 mL, 10.79 mmol) was added dropwise over 10 min to a solution of indole (1.28 g, 10.79 mmol) in THF (6 mL) at 0 °C. The solution was stirred at 0–2 °C for 30 min. 2,4,5-Trichloropyrimidine (1 g, 5.40 mmol) was added dropwise, resulting in a yellow solution. The ice bath was removed, and the solution was stirred at ambient temperature for 1 h, resulting in a red solution. The temperature was elevated to 60 °C, and the mixture was stirred at 60 °C for 1.5 h. The mixture was cooled to 25 °C, and acetic acid (634 μL , 11.06 mmol) was added dropwise. Water (9.90 mL) and THF (2 mL) were added, and the mixture was stirred for 20 min at 60 °C, resulting in a biphasic solution. The layers were partitioned, and heptane (11 mL) was added to the organic solution, resulting in the crystallization of a solid. The solid was collected by filtration, washed with heptane (2 mL), and dried in a vacuum oven to yield 3-(2,5-dichloropyrimidin-4-yl)-1H-indole (1.015 g, 66%) as a yellow solid. ^1H NMR ($\text{DMSO}-d_6$) δ 7.24–7.32 (2H, m), 7.55–7.58 (1H, m), 8.52–8.55 (1H, m), 8.71–8.73 (2H, m), 12.24 (1H, s); ES+ m/z : ($\text{M} + \text{H}$) $^+$ 264/266.

4-Fluoro-2-methoxy-1-nitrobenzene (62).

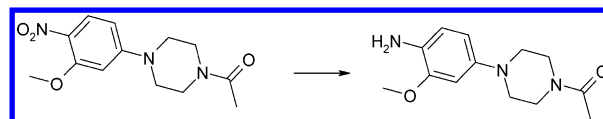


Potassium carbonate (44 g, 318.27 mmol) and 5-fluoro-2-nitrophenol (50 g, 318.27 mmol) dissolved in acetone (750 mL) were stirred under argon for 30 min, and methyl iodide (19.81 mL, 318.27 mmol) was added dropwise. The resulting solution was stirred at 60 °C overnight, allowed to cool to room temperature, and concentrated to dryness. Water (500 mL) was added, and the resulting mixture was extracted with EtOAc (3 \times 200 mL). The organic layers were combined, washed with a 1 M aqueous solution of NaOH (2 \times 200 mL) and brine (200 mL), dried (MgSO_4), and concentrated to afford the crude product as an oil, which was crystallized to give 4-fluoro-2-methoxy-1-nitrobenzene (53.8 g, 99%) as a clear beige solid. ^1H NMR ($\text{DMSO}-d_6$) δ 3.93 (3H, s), 6.93–6.98 (1H, m), 7.28–7.31 (1H, m), 7.99–8.02 (1H, m). No ionization in LC–MS. 1-[4-(3-Methoxy-4-nitrophenyl)piperazin-1-yl]ethanone (63).



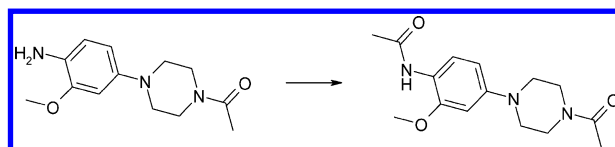
1-Acetylpiperazine (12.36 g, 96.42 mmol) and DIPEA (18.32 mL, 105.19 mmol) were added to a stirred solution of 4-fluoro-2-methoxy-1-nitrobenzene (62) (15 g, 87.65 mmol) dissolved in DMA (45 mL) under argon. The resulting solution was stirred at 90 °C overnight. The reaction mixture was allowed to cool to room temperature and quenched with water (500 mL). The aqueous layer was extracted with EtOAc ($\times 3$). The combined organic layers were washed with water ($\times 2$) and brine, dried (MgSO_4), and concentrated to afford 1-[4-(3-methoxy-4-nitrophenyl)piperazin-1-yl]ethanone (22.0 g, 90%) as a yellow solid. ^1H NMR (CDCl_3) δ 2.15 (3H, s), 3.43 (4H, dt), 3.67 (2H, t), 3.80 (2H, t), 6.33 (1H, d), 6.42 (1H, dd), 8.00 (1H, d); ES+ m/z : ($\text{M} + \text{H}$) $^+$ 280.35.

1-[4-(4-Amino-3-methoxyphenyl)piperazin-1-yl]ethanone (64).



A suspension of 1-[4-(3-methoxy-4-nitrophenyl)piperazin-1-yl]ethanone (7 g, 25.06 mmol) and platinum oxide (0.398 g, 1.75 mmol) in EtOH (200 mL) at 25 °C was stirred under 1.3 bar hydrogen at 25 °C for 3 h. The resulting suspension was filtered through Dicalite Speed Plus, and the filtrate was concentrated to dryness to afford 1-[4-(4-amino-3-methoxyphenyl)piperazin-1-yl]ethanone (6.19 g, 99%) as a purple solid. ^1H NMR (400 MHz, $\text{DMSO}-d_6$) δ 2.03 (3H, s), 2.87 (2H t, $J = 5.2$ Hz), 2.94 (2H t, $J = 5.2$ Hz), 3.53–3.57 (4H, m), 3.75 (3H, s), 4.28 (2H, s), 6.30–6.33 (1H, m), 6.52–6.54 (2H, m); ES+ m/z : ($\text{M} + \text{H}$) $^+$ 250.27.

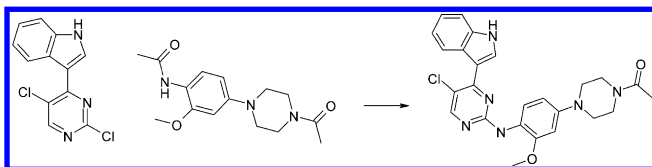
N-[4-(4-Acetylpiperazin-1-yl)-2-methoxyphenyl]acetamide (65).



1-[4-(4-Amino-3-methoxyphenyl)piperazin-1-yl]ethanone (64) (3 g, 12.03 mmol) was added to a stirred mixture of acetic

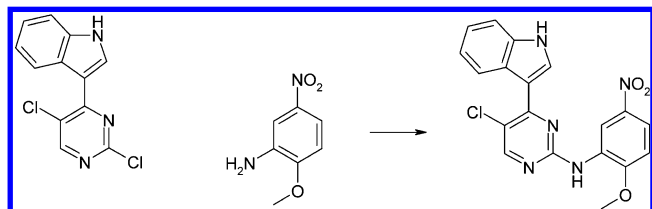
anhydride (7.49 mL, 79.42 mmol) and acetic acid (3.10 mL, 54.15 mmol). The resulting deep-blue solution was stirred at 25 °C for 1 h. The reaction mixture was then diluted in Et₂O (500 mL) under stirring. The precipitate was collected by filtration and washed with Et₂O to give *N*-(4-(4-acetylpiperazin-1-yl)-2-methoxyphenyl)acetamide (2.55 g, 73%) as a clear purple solid. ¹H NMR (DMSO-*d*₆) δ 2.02 (3H, s), 2.06 (3H, s), 3.09 (4H, ddd), 3.58 (4H, m), 3.81 (3H, s), 6.45 (1H, d), 6.63 (1H, s), 7.61 (1H, d), 8.92 (1H, s); ES+ *m/z*: (M + H)⁺ 292.36.

1-[4-[4-[[5-Chloro-4-(1*H*-indol-3-yl)pyrimidin-2-yl]amino]-3-methoxyphenyl]piperazin-1-yl]ethanone (**7**).



3-(2,5-Dichloropyrimidin-4-yl)-1*H*-indole (**61**) (0.25 g, 0.95 mmol), 1-(4-(4-amino-3-methoxyphenyl)piperazin-1-yl)ethanone (0.271 g, 0.95 mmol), and *p*-toluene sulfonic acid monohydrate (0.552 mL, 2.84 mmol) in *n*-pentanol (4 mL)/NMP (1 mL) were stirred at 150 °C for 1 h. The reaction mixture was filtered and concentrated in vacuo, and the residue was purified by reverse-phase HPLC (acetonitrile/water/0.1% TFA) using an Atlantis Prep T3 OBD column to afford 1-[4-[4-[[5-chloro-4-(1*H*-indol-3-yl)pyrimidin-2-yl]amino]-3-methoxyphenyl]piperazin-1-yl]ethanone (138 mg, 31%) as a white solid and the deacetylated product as a white solid (42 mg, 10%). ¹H NMR (DMSO-*d*₆) δ 2.07 (3H, s), 3.13–3.39 (4H, m), 3.65 (4H, d), 3.73–3.88 (3H, m), 6.63 (1H, dd), 6.82 (1H, d), 7.01 (1H, t), 7.14–7.23 (1H, m), 7.47 (1H, d), 7.54 (1H, d), 8.28 (1H, d), 8.34 (1H, s), 8.54 (1H, d), 11.94 (1H, br s); ¹³C NMR (DMSO-*d*₆) δ 21.10, 40.70, 45.49, 49.02, 49.35, 55.46, 100.86, 107.30, 110.88, 111.55, 114.07, 120.36, 120.70, 122.24, 123.17, 125.71, 126.12, 130.71, 135.87, 149.04, 153.11, 157.11, 157.75, 159.39, 168.17; HRMS–ESI (*m/z*): [M + H]⁺ calcd for C₂₅H₂₅O₂N₆Cl, 477.17969; found, 477.18003.

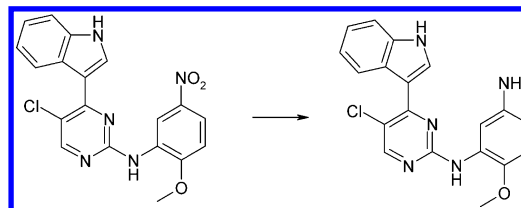
Synthesis of Compound 9. 5-Chloro-4-(1*H*-indol-3-yl)-*N*-(2-methoxy-5-nitrophenyl)pyrimidin-2-amine (**66**).



2-Methoxy-5-nitroaniline (0.971 g, 5.77 mmol), *p*-toluene sulfonic acid monohydrate (2.197 g, 11.55 mmol), and 3-(2,5-dichloropyrimidin-4-yl)-1*H*-indole (**61**) (1.525 g, 5.77 mmol) were heated at 120 °C in 2-pentanol (20 mL) for 24 h. The reaction mixture was evaporated to dryness, redissolved in DCM (50 mL) and MeOH (5 mL), and washed sequentially with saturated NaHCO₃ (25 mL), water (25 mL), and saturated brine (25 mL). The organic layer was dried (MgSO₄) and evaporated to afford the crude product. The resultant solid was triturated with DCM/MeOH (9:1), filtered, and washed with DCM to give 5-chloro-4-(1*H*-indol-3-yl)-*N*-(2-methoxy-5-nitrophenyl)pyrimidin-2-amine (1.20 g, 53%) as a yellow solid (1.2 g, 53%). ¹H NMR (DMSO-*d*₆) δ 4.01 (3H, s), 6.95–7.10 (1H, m), 7.21 (1H, t), 7.32 (1H, d), 7.50 (1H, d), 8.03–8.12 (1H, m), 8.32–8.42 (1H, m),

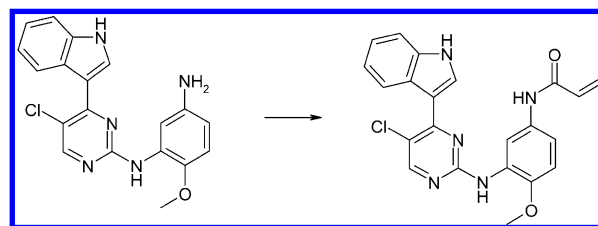
8.49–8.58 (2H, m), 8.62 (1H, s), 8.93 (1H, d), 11.93 (1H, s); ES+ *m/z*: (M + H)⁺ 396.13.

N'-[5-Chloro-4-(1*H*-indol-3-yl)pyrimidin-2-yl]-4-methoxybenzene-1,3-diamine (**67**).



5-Chloro-4-(1*H*-indol-3-yl)-*N*-(2-methoxy-5-nitrophenyl)pyrimidin-2-amine (**66**) (1.2 g, 3.03 mmol), iron (1.016 g, 18.19 mmol), and ammonium chloride (0.114 g, 2.12 mmol) were heated in ethanol (15 mL) and water (5 mL) at reflux for 3 h. The mixture was cooled and concentrated to a thick slurry. DCM (100 mL), MeOH (5 mL), and water were added, and the mixture stirred for 15 min and filtered. The filtrate layers were separated, and the aqueous layer was re-extracted with DCM. The combined organics were dried (MgSO₄) and concentrated. The crude product was purified by flash silica chromatography, eluting with 1–5% MeOH in DCM. Pure fractions were evaporated to dryness to afford *N*1-(5-chloro-4-(1*H*-indol-3-yl)pyrimidin-2-yl)-6-methoxybenzene-1,3-diamine (0.825 g, 74%) as a white/pale-yellow solid. ¹H NMR (DMSO-*d*₆) δ 3.71 (3H, s), 4.55 (2H, s), 6.36 (1H, dd), 6.80 (1H, d), 7.08–7.13 (1H, m), 7.17–7.23 (1H, m), 7.26 (1H, d), 7.49 (1H, d), 8.13 (1H, s), 8.39 (1H, s), 8.42 (1H, d), 8.49 (1H, d), 11.85 (1H, s); ES+ *m/z*: (M + H)⁺ 366.17

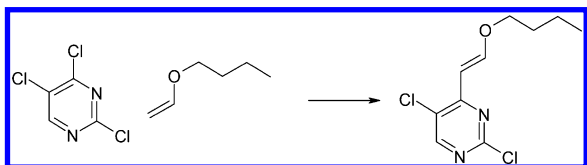
N-[3-[[5-Chloro-4-(1*H*-indol-3-yl)pyrimidin-2-yl]amino]-4-methoxyphenyl]prop-2-enamide (**9**).



Acryloyl chloride (0.040 mL, 0.49 mmol) was added dropwise to *N'*-[5-chloro-4-(1*H*-indol-3-yl)pyrimidin-2-yl]-4-methoxybenzene-1,3-diamine (**67**) (180.2 mg, 0.49 mmol) and DIPEA (0.146 mL, 0.54 mmol) in THF (5 mL) at 0 °C under nitrogen. The resulting suspension was stirred at 0 °C for 2 h and then allowed to warm to room temperature. The reaction mixture was diluted with water (15 mL) and extracted with DCM (40 mL). The organics were washed sequentially with saturated Na₂CO₃ (20 mL) and saturated brine (20 mL). The organic layer was dried (MgSO₄) and evaporated to afford the crude product. The crude product was purified by flash silica chromatography, eluting with 1–8% MeOH in DCM. Pure fractions were evaporated to dryness to afford *N*-[3-[[5-chloro-4-(1*H*-indol-3-yl)pyrimidin-2-yl]amino]-4-methoxyphenyl]prop-2-enamide (125 mg, 60%) as a pale-brown solid. ¹H NMR (DMSO-*d*₆) δ 3.80 (3H, s), 5.70 (1H, dd), 6.22 (1H, dd), 6.40 (1H, dd), 6.99 (1H, t), 7.06 (1H, d), 7.16 (1H, t), 7.46 (1H, d), 7.55 (1H, dd), 8.05 (1H, d), 8.33 (1H, d), 8.40 (2H, s), 8.51 (1H, d), 9.97 (1H, s), 11.85 (1H, s); ¹³C NMR (DMSO-*d*₆) δ 55.77, 110.74, 111.27, 111.61, 114.97, 115.71, 116.06, 120.53, 122.28, 123.00, 126.04, 128.16, 131.02, 131.90, 131.99, 135.93, 147.87, 157.14, 158.02, 158.70, 162.67;

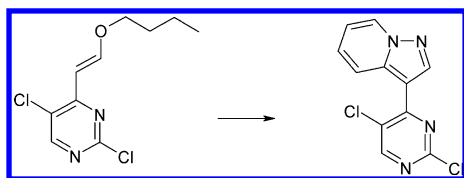
HRMS–ESI (m/z): $[M + H]^+$ calcd for $C_{22}H_{19}O_2N_3Cl$, 420.12198; found, 420.12218.

Synthesis of Compound 15. (*E*)-4-(2-Butoxyvinyl)-2,5-dichloropyrimidine (**68**).



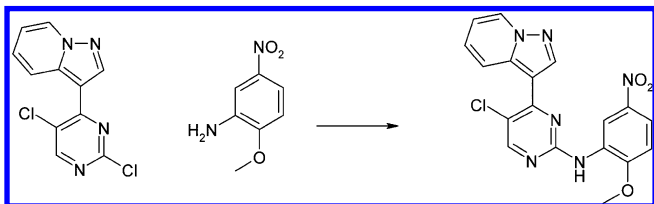
Triethylamine (80 mL, 572.45 mmol), butyl vinyl ether (74.1 mL, 572.45 mmol), and palladium(II) acetate (4.28 g, 19.08 mmol) were added to a stirred solution of 2,4,5-trichloropyrimidine (100 g, 545.2 mmol) in poly(ethylene glycol) 200 (600 mL, 545.2 mmol) under nitrogen. The mixture was stirred at 80 °C for 70 min and then cooled to room temperature. The mixture was extracted with Et_2O (4 × 1 L). The combined organics were washed with water (2 × 1 L) and brine (1 L). The solution was then dried ($MgSO_4$) and concentrated in vacuo. Purification by flash silica chromatography and elution with 0–40% DCM in isohexane afforded (*E*)-4-(2-butoxyvinyl)-2,5-dichloropyrimidine (**68**; 2.8 g, 51%) as a light-yellow oil. 1H NMR ($DMSO-d_6$) δ 0.91 (3H, t), 1.33–1.42 (2H, m), 1.62–1.69 (2H, m), 4.11 (2H, t), 6.05 (1H, d), 8.04 (1H, d), 8.62 (1H, s); ES+ m/z : $(M + H)^+$ 247.30

3-(2,5-Dichloropyrimidin-4-yl)pyrazolo[1,5-*a*]pyridine (**69**).



To a stirred solution of (*E*)-4-(2-butoxyvinyl)-2,5-dichloropyrimidine (**68**) (8 g, 32.37 mmol) in DMA (100 mL) was added 1-aminopyridinium iodide (7.19 g, 32.37 mmol) followed by K_2CO_3 (11.19 g, 80.93 mmol). The mixture was stirred at 110 °C for 5 h. After cooling to room temperature, the mixture became solid. The mixture was diluted with EtOAc and a small amount of MeOH and was then washed with water followed by saturated brine. The mixture was filtered to remove the solid from the phase interface. This solid contained some desired product. The solid was dissolved in EtOAc/MeOH and was combined with the organic extract. Purification by flash silica chromatography and elution with 20–70% EtOAc in heptane provided 3-(2,5-dichloropyrimidin-4-yl)pyrazolo[1,5-*a*]pyridine (**69**; 2.86 g, 33%) as an orange solid. 1H NMR ($DMSO-d_6$) δ 7.28 (1H, td), 7.73 (1H, ddd), 8.57 (1H, dt), 8.81 (1H, s), 8.97 (1H, dt), 9.09 (1H, s); (1H, d), 9.54 (1H, t); ES+ m/z : $(M + H)^+$ 265.

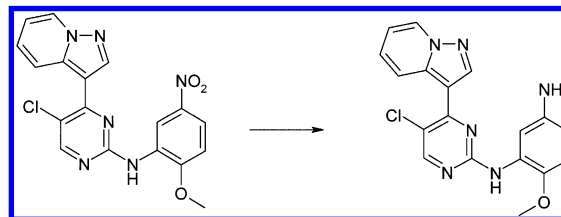
5-Chloro-*N*-(2-methoxy-5-nitrophenyl)-4-(pyrazolo[1,5-*a*]pyridin-3-yl)pyrimidin-2-amine (**70**).



4-Methylbenzenesulfonic acid hydrate (15.79 g, 82.99 mmol) was added in one portion to 2-methoxy-5-nitroaniline (12.69 g,

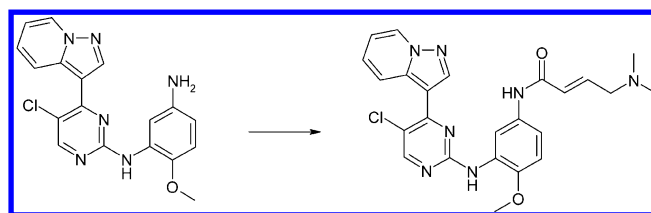
75.44 mmol) and 3-(2,5-dichloropyrimidin-4-yl)pyrazolo[1,5-*a*]pyridine (20 g, 75.44 mmol) in 2-pentanol (300 mL). The resulting mixture was stirred at 100 °C for 2 days. The resulting precipitate was collected by filtration, washed with 2-pentanol (5 mL), and dried in vacuo to give a yellow solid. The solid was slurried in acetonitrile, filtered, and dried in vacuo to give 5-chloro-*N*-(2-methoxy-5-nitrophenyl)-4-(pyrazolo[1,5-*a*]pyridin-3-yl)pyrimidin-2-amine (22.97 g, 77%). 1H NMR ($DMSO-d_6$, 100 °C) δ 4.05 (3H, s), 7.15 (1H, t), 7.33 (1H, d), 7.43 (1H, t), 8.04 (1H, dd), 8.45–8.51 (2H, m), 8.57 (1H, s), 8.81 (1H, d), 8.93–8.95 (2H, m); ES+ m/z : $(M + H)^+$ 397.

*N*1-[5-Chloro-4-(pyrazolo[1,5-*a*]pyridin-3-yl)pyrimidin-2-yl]-6-methoxybenzene-1,3-diamine (**71**).



5-Chloro-*N*-(2-methoxy-5-nitrophenyl)-4-(pyrazolo[1,5-*a*]pyridin-3-yl)pyrimidin-2-amine (22.9 g, 57.71 mmol), iron (powder, 325 mesh, 19.34 g, 346.28 mmol), and an NH_4Cl solution (1.412 mL, 40.40 mmol) were added to a mixture of EtOH (1145 mL) and water (382 mL). The mixture was then heated at reflux for 1 h and then cooled and concentrated to a thick slurry. This residue was triturated with EtOAc (450 mL) and a small amount of saturated $NaHCO_3$ and then filtered. The isolated solid was washed with water (250 mL) and then slurried with 10% MeOH/DCM (1 L) for 15 min. The mixture was filtered, and the isolated solid was reslurried with 10% MeOH/DCM (250 mL) and filtered. The combined filtrates were separated from the residual water, dried (Na_2SO_4), and concentrated in vacuo. The resulting solid was suspended in MeOH (150 mL), filtered, washed with MeOH and Et_2O , and dried on the filter to provide *N*1-[5-chloro-4-(pyrazolo[1,5-*a*]pyridin-3-yl)pyrimidin-2-yl]-6-methoxybenzene-1,3-diamine (**71**; 17.1 g, 81%) as a yellow powder. 1H NMR ($DMSO-d_6$) δ 3.68 (3H, s), 4.63 (2H, s), 6.41 (1H, dd), 6.82 (1H, d), 7.06 (1H, d), 7.13 (1H, td), 7.38–7.45 (1H, m), 8.39 (1H, s), 8.42 (1H, s), 8.48 (1H, d), 8.84 (1H, d), 8.95 (1H, s); ES+ m/z : $(M + H)^+$ 367.

(*E*)-*N*-[3-[5-Chloro-4-(pyrazolo[1,5-*a*]pyridin-3-yl)pyrimidin-2-ylamino]-4-methoxyphenyl]-4-(dimethylamino)but-2-enamide (**15**).

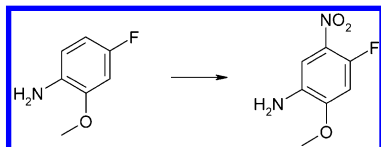


DIPEA (0.119 mL, 0.68 mmol), (*E*)-4-bromobut-2-enoic acid (49.5 mg, 0.30 mmol), and HATU (114 mg, 0.30 mmol) were added to a stirred solution of *N*1-[5-chloro-4-(pyrazolo[1,5-*a*]pyridin-3-yl)pyrimidin-2-yl]-6-methoxybenzene-1,3-diamine (**71**) (100 mg, 0.27 mmol) in DMF (10 mL) at 0 °C. The mixture was stirred at 1 °C under nitrogen for 2 h, allowed to warm to room temperature, and stirred for a further 2 h. The mixture was then recooled to 0 °C, and dimethylamine (2 M in THF, 2.73 mL, 5.45 mmol) was added. The mixture was stirred at 1 °C for 5 min, allowed to warm to room temperature, and

stirred for a further 3 h. The mixture was then diluted with EtOAc (50 mL) and was washed with water (2 × 50 mL) and saturated brine (50 mL). The solution was dried (MgSO₄) and concentrated in vacuo. Purification by flash silica chromatography and elution with 0–10% MeOH in DCM (containing 1% aqueous NH₃) provided (*E*)-*N*-{3-[5-chloro-4-(pyrazolo[1,5-*a*]pyridin-3-yl)pyrimidin-2-ylamino]-4-methoxyphenyl}-4-(dimethylamino)but-2-enamide (30 mg, 23%) as an orange solid. ¹H NMR (DMSO-*d*₆) δ 2.19 (6H, s), 3.06 (2H, d), 3.79 (3H, s), 6.23 (1H, d), 6.69 (1H, dt), 7.06–7.15 (2H, m), 7.29–7.35 (1H, m), 7.56 (1H, dd), 7.96 (1H, d), 8.42 (1H, d), 8.46 (1H, s), 8.73 (1H, s), 8.86 (1H, d), 8.99 (1H, s), 9.97 (1H, s); ¹³C NMR (DMSO-*d*₆) δ 42.05, 55.77, 56.82, 106.97, 111.52, 114.37, 114.77, 116.28, 116.66, 120.60, 126.88, 128.00, 129.49, 130.89, 131.62, 132.22, 139.33, 143.38, 148.54, 155.61, 157.80, 158.76, 161.48. HRMS–ESI (*m/z*): [M + H]⁺ calcd for C₂₄H₂₄O₂N₇Cl, 478.17502; found, 478.17528.

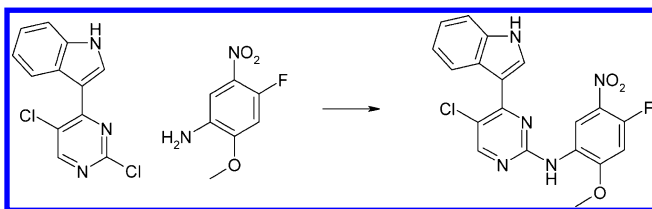
(*E*)-*N*-{3-[5-Chloro-4-(pyrazolo[1,5-*a*]pyridin-3-yl)pyrimidin-2-ylamino]-4-methoxyphenyl}-4-(dimethylamino)but-2-enamide (15) Mesylate Salt. (*E*)-*N*-{3-[5-Chloro-4-(pyrazolo[1,5-*a*]pyridin-3-yl)pyrimidin-2-ylamino]-4-methoxyphenyl}-4-(dimethylamino)but-2-enamide (15) (50 mg, 0.104 mmol) was dissolved in hot MeCN (5 mL) and combined with a solution of methanesulfonic acid (10 mg, 0.104 mmol) in MeCN (1 mL). The resultant mixture was then stirred at room temperature for 24 h. The resulting off-white solid was collected by filtration and analyzed by XRD and thermal methods. On analysis, this solid gave a different X-ray powder diffraction pattern from that of the starting material, indicating a new crystalline phase had been formed. This phase was shown by differential scanning calorimetry to have an onset of melting of around 235 °C.

Synthesis of Compound 58. 4-Fluoro-2-methoxy-5-nitroaniline (72).



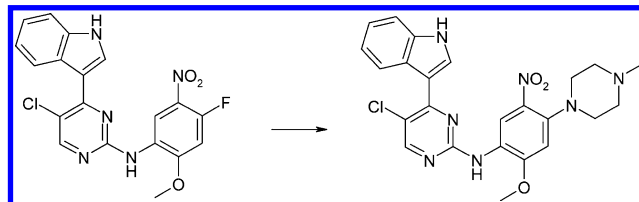
4-Fluoro-2-methoxyaniline (2.4 g, 17.00 mmol) was added portionwise to concd H₂SO₄ (15 mL) and cooled in a ice-water bath, keeping the temperature below 15 °C. The mixture was stirred until all of the solid that formed had dissolved. Potassium nitrate (0.815 mL, 17.00 mmol) was added portionwise such that the temperature was maintained below 10 °C. The mixture was stirred overnight and then poured onto ice/water. The mixture was basified with concd NH₄OH. The solid was filtered off and then dissolved in DCM, washed with water, dried (Na₂SO₄), and concentrated onto silica. The crude product was purified by flash silica chromatography and eluted with a gradient of 50–100% DCM in heptane. Pure fractions were evaporated to dryness to afford 4-fluoro-2-methoxy-5-nitroaniline (2.450 g, 77%) as a yellow crystalline solid. ¹H NMR (DMSO-*d*₆) δ 3.91 (3H, s), 5.21 (2H, s), 7.03 (1H, d), 7.35 (1H, d); ES+ *m/z*: (M + H)⁺ 187.4.

5-Chloro-*N*-(4-fluoro-2-methoxy-5-nitrophenyl)-4-(1*H*-indol-3-yl)pyrimidin-2-amine (73).



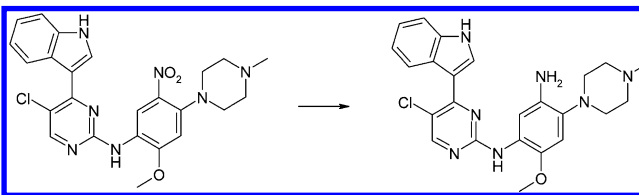
3-(2,5-Dichloropyrimidin-4-yl)-1*H*-indole (61) (7.5 g, 28.40 mmol), 4-fluoro-2-methoxy-5-nitroaniline (72) (5.55 g, 29.82 mmol), and *p*-toluenesulfonic acid monohydrate (5.94 g, 31.24 mmol) were heated at 120 °C in 2-pentanol (210 mL) for 18 h. The mixture was cooled and filtered. The solid was washed with MeOH and Et₂O and dried on the filter to give 5-chloro-*N*-(4-fluoro-2-methoxy-5-nitrophenyl)-4-(1*H*-indol-3-yl)pyrimidin-2-amine (7.28 g, 62%). ¹H NMR (DMSO-*d*₆) δ 3.98 (3H, s), 6.97–7.05 (1H, m), 7.17–7.24 (1H, m), 7.40 (1H, d), 7.49 (1H, dd), 8.29 (1H, d), 8.49 (1H, s), 8.52 (1H, d), 8.68 (1H, d), 8.71 (1H, s), 11.92 (1H, s); ES+ *m/z*: (M + H)⁺ 414.1.

5-Chloro-4-(1*H*-indol-3-yl)-*N*-[2-methoxy-4-(4-methylpiperazin-1-yl)-5-nitrophenyl]pyrimidin-2-amine (74).



1-Methylpiperazine (492 μL, 4.44 mmol) was added to a suspension of 5-chloro-*N*-(4-fluoro-2-methoxy-5-nitrophenyl)-4-(1*H*-indol-3-yl)pyrimidin-2-amine (73) (612 mg, 1.48 mmol), and the reaction was stirred at 120 °C for 1 h. The reaction mixture was evaporated to dryness, redissolved in DCM (25 mL), and washed sequentially with water (2 × 25 mL) and saturated brine (25 mL). The organic layer was dried (MgSO₄) and evaporated to afford the crude product. The crude product was purified by flash silica chromatography, with an elution gradient of 1–10% MeOH in DCM. Pure fractions were evaporated to dryness, the resulting gum was dissolved in EtOH (25 mL), and a solid precipitated. The solid was collected by filtration and washed with EtOH and Et₂O to give 5-chloro-4-(1*H*-indol-3-yl)-*N*-[2-methoxy-4-(4-methylpiperazin-1-yl)-5-nitrophenyl]pyrimidin-2-amine (365 mg, 50%) as a yellow solid. ¹H NMR (DMSO-*d*₆) δ 2.26 (3H, s), 2.47–2.55 (4H, m), 3.07–3.13 (4H, m), 3.93 (3H, s), 6.85 (1H, s), 6.99 (1H, t), 7.16–7.22 (1H, m), 7.48 (1H, d), 8.26 (1H, d), 8.36 (1H, s), 8.42 (1H, d), 8.51 (1H, s), 8.54 (1H, s), 11.88 (1H, s); ES+ *m/z*: (M + H)⁺ 494.5.

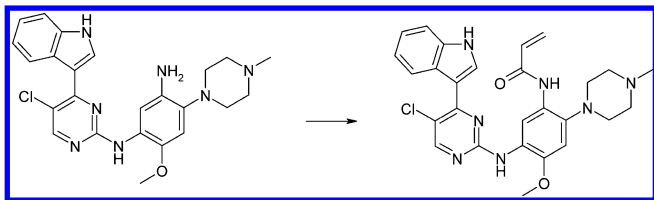
N'-[5-Chloro-4-(1*H*-indol-3-yl)pyrimidin-2-yl]-4-methoxy-6-(4-methylpiperazin-1-yl)benzene-1,3-diamine (75).



5-Chloro-4-(1*H*-indol-3-yl)-*N*-[2-methoxy-4-(4-methylpiperazin-1-yl)-5-nitrophenyl]pyrimidin-2-amine (74) (350 mg, 0.71 mmol), iron (237 mg, 4.25 mmol), and ammonium chloride (26.5 mg, 0.50 mmol) were heated in EtOH (24 mL) and water (8 mL) at reflux for 2 h. The mixture was cooled and concentrated to a thick slurry. DCM (100 mL) and MeOH (10 mL) were added, and the mixture was stirred for 15 min and filtered. The filtrate was dried (MgSO₄) and concentrated. The crude product was purified by flash silica chromatography, eluting with 1–5% MeOH/NH₃ in DCM. Pure fractions were evaporated to dryness to afford *N*'-[5-chloro-4-(1*H*-indol-3-yl)pyrimidin-2-yl]-4-methoxy-6-(4-methylpiperazin-1-yl)benzene-1,3-diamine

(288 mg, 88%) as a pale-yellow foam. ^1H NMR (DMSO- d_6) δ 2.26 (3H, s), 2.47–2.56 (4H, m), 2.88 (4H, t), 3.70 (3H, s), 4.29 (2H, d), 6.72 (1H, s), 7.04 (1H, t), 7.14 (1H, s), 7.15–7.22 (1H, m), 7.46 (1H, d), 8.18 (1H, s), 8.35 (2H, d), 8.48 (1H, d), 11.81 (1H, s); ES+ m/z : (M + H) $^+$ 464.5.

N-[5-[[5-Chloro-4-(1*H*-indol-3-yl)pyrimidin-2-yl]amino]-4-methoxy-2-(4-methylpiperazin-1-yl)phenyl]prop-2-enamide (**58**).



Acryloyl chloride (1 M in THF, 0.621 mL, 0.62 mmol) was added dropwise to *N*-[5-chloro-4-(1*H*-indol-3-yl)pyrimidin-2-yl]-4-methoxy-6-(4-methylpiperazin-1-yl)benzene-1,3-diamine (**75**) (288 mg, 0.62 mmol) and DIPEA (0.119 mL, 0.68 mmol) in THF (15 mL) at 0 °C under nitrogen. The resulting suspension was stirred at 0 °C for 1 h and then allowed to warm to room temperature. The reaction mixture was diluted with water (15 mL) and reduced in vacuo. The resultant crude product was dissolved in DCM (20 mL) and MeOH (5 mL) and washed with water and saturated brine. The organic layer was dried (MgSO₄) and evaporated. The crude product was purified by flash silica chromatography, with an elution gradient of 1–8% MeOH/NH₃ in DCM. Pure fractions were evaporated to dryness. The product was dissolved in DCM, and a beige solid precipitated from the solution. This solid was diluted with Et₂O and filtered, washed with further Et₂O, and dried to give *N*-[5-[[5-chloro-4-(1*H*-indol-3-yl)pyrimidin-2-yl]amino]-4-methoxy-2-(4-methylpiperazin-1-yl)phenyl]prop-2-enamide (134 mg, 42%) as a beige solid. ^1H NMR (DMSO- d_6) δ 2.27 (3H, s), 2.53–2.59 (4H, m), 2.87–2.94 (4H, m), 3.79 (3H, s), 5.70 (1H, d), 6.17 (1H, dd), 6.60 (1H, dd), 6.89 (1H, s), 7.01 (1H, t), 7.16 (1H, t), 7.45 (1H, d), 8.20 (1H, s), 8.27 (1H, d), 8.35 (1H, s), 8.43 (1H, s), 8.49 (1H, d), 8.96 (1H, s), 11.81 (1H, s); ^{13}C NMR (DMSO- d_6) δ 45.74, 51.23, 54.77, 55.72, 103.74, 110.82, 111.53, 114.43, 120.14, 120.48, 122.20, 123.03, 123.42, 124.46, 125.90, 126.05, 130.85, 132.23, 135.86, 141.31, 149.80, 157.15, 157.86, 159.13, 162.76; HRMS–ESI (m/z): [M + H] $^+$ calcd for C₂₇H₂₈O₂N₇Cl, 518.20636; found, 518.20658.

The full synthesis and characterization of the novel compounds is detailed in the Supporting Information. Additional compounds reported from the reactivity data set from the alternative templates and alternative covalent functionality were synthesized by exploiting the modular approaches reported in this manuscript in addition to using routes subsequently disclosed in the literature.^{43,51} Compounds used as model systems (Table 7) were either available in our compound collection, purchased from commercial sources, or synthesized from commonly available building blocks.

Measuring Compound Reactivity. Fifty micromolar of compound was reacted with an excess of glutathione (4.6 mM GSH) in phosphate buffer at pH 7.4 and 37 °C for 24 h.^{36,37} The reaction was followed by monitoring the loss of the parent by LC–UV–MS, and the data were fitted to first-order kinetics from which the pseudo-first-order rate constant was produced and subsequently k_{GSH} . Reaction of *para*-nitrobenzylchloride (PNBC) with glutathione was used as a positive control for the assay (Log k_{GSH} = $-1.747 \text{ mol}^{-1} \text{ s}^{-1}$, SD 0.077, and $n = 24$).

In Vivo Xenograft Antitumor Studies. All animal experiments were conducted in full accordance with the U.K. Home Office Animal (Scientific Procedures) Act 1986. Xenografts were established by subcutaneous cell implantation into the left flank of either athymic (Swiss nu/nu; Alpk; H1975 and A431) or severe-combined

immunodeficiency (SCID) mice (SCID/CB17; PC9). Animals were randomized into treatment groups of 4–10 mice, with a group mean tumor size of ~0.2–0.4 cm³. Mice were then treated once daily by oral gavage with either vehicle or inhibitor for up to 14 days. Tumor growth inhibition (TGI) was calculated for compound-treated groups compared to vehicle controls (p values provided), where a TGI > 100% indicates tumor regression from the size of the initial tumor. Statistical significance was evaluated using a one-tailed t test.

■ ASSOCIATED CONTENT

§ Supporting Information

Reaction of compound **38** in buffer, structure of compound **60**, chemical structures of the compounds in Tables 7 and 8, reaction of compounds with glutathione with and without human glutathione-S-transferase, and kinase selectivity of compound **15**. Methods of protein–ligand docking and full compound synthesis and characterization. This material is available free of charge via the Internet at <http://pubs.acs.org>.

■ AUTHOR INFORMATION

Corresponding Author

*Phone: +44 (0)1625 519045. E-mail: richard.a.ward@astrazeneca.com.

Notes

The authors declare no competing financial interest.

■ ACKNOWLEDGMENTS

We thank all of our colleagues at AstraZeneca, past and present, who have contributed to this work. We also thank Proteros for supplying the described X-ray crystal structure and Millipore for providing the early biochemical data. Finally, we thank Dr. Andy Barker who was instrumental in supporting the early efforts on this project.

■ DEDICATION

[‡]This manuscript is dedicated to the late Peter Smith.

■ ABBREVIATIONS USED

EGFR, epidermal growth factor receptor; NSCLC, non-small cell lung cancer; TKI, tyrosine kinase inhibitor; QSPR, quantitative structure property relationship; GSH, glutathione; PK, pharmacokinetics; WT, wild type; AM, activating mutant; DM, double mutant; LLE, ligand lipophilicity efficiency; LC–MS, liquid chromatography–mass spectrometry; QM/MM, quantum mechanical/molecular modeling; SAR, structure–activity relationships; CRO, contract research organization

■ REFERENCES

- (1) Normanno, N.; De Luca, A.; Bianco, C.; Strizzi, L.; Mancino, M.; Maiello, M. R.; Carotenuto, A.; De Feo, G.; Caponigro, F.; Salomon, D. S. Epidermal growth factor receptor (EGFR) signaling in cancer. *Gene* **2006**, *366*, 2–16.
- (2) Sharma, S. V.; Bell, D. W.; Settleman, J.; Haber, D. A. Epidermal growth factor receptor mutations in lung cancer. *Nat. Rev. Cancer* **2007**, *7*, 169–181.
- (3) Pao, W.; Chmielecki, J. Rational, biologically based treatment of EGFR-mutant non-small-cell lung cancer. *Nat. Rev. Cancer* **2010**, *10*, 760–774.
- (4) Maemondo, M.; Inoue, A.; Kobayashi, K.; Sugawara, S.; Oizumi, S.; Isobe, H.; Gemma, A.; Harada, M.; Yoshizawa, H.; Kinoshita, I.; Fujita, Y.; Okinaga, S.; Hirano, H.; Yoshimori, K.; Harada, T.; Ogura, T.; Ando, M.; Miyazawa, H.; Tanaka, T.; Saijo, Y.; Hagiwara, K.; Morita, S.; Nukiwa, T. Gefitinib or chemotherapy for non-small-cell

lung cancer with mutated EGFR. *N. Engl. J. Med.* **2010**, *362*, 2380–2388.

(5) Kobayashi, S.; Boggon, T. J.; Dayaram, T.; Janne, P. A.; Kocher, O.; Meyerson, M.; Johnson, B. E.; Eck, M. J.; Tenen, D. G.; Halmos, B. EGFR mutation and resistance of non-small-cell lung cancer to gefitinib. *N. Engl. J. Med.* **2005**, *352*, 786–792.

(6) Yun, C.; Mengwasser, K. E.; Toms, A. V.; Woo, M. S.; Greulich, H.; Wong, K.; Meyerson, M.; Eck, M. J. The T790M mutation in EGFR kinase causes drug resistance by increasing the affinity for ATP. *Proc. Natl. Acad. Sci. U.S.A.* **2008**, *105*, 2070–2075.

(7) Shepherd, F. A.; Pereira, J. R.; Ciuleanu, T.; Tan, E. H.; Hirsh, V.; Thongprasert, S.; Campos, D.; Maoleekoonpiroj, S.; Smylie, M.; Martins, R.; van Kooten, M.; Dediu, M.; Findlay, B.; Tu, D.; Johnston, D.; Bezjak, A.; Clark, G.; Santabarbara, P.; Seymour, L. Erlotinib in previously treated non-small-cell lung cancer. *N. Engl. J. Med.* **2005**, *353*, 123–132.

(8) Zhang, Z.; Stiegler, A. L.; Boggon, T. J.; Kobayashi, S.; Halmos, B. EGFR-mutated lung cancer: A paradigm of molecular oncology. *Oncotargets Ther.* **2010**, *1*, 497–514.

(9) Sogabe, S.; Kawakita, Y.; Igaki, S.; Iwata, H.; Miki, H.; Cary, D. R.; Takagi, T.; Takagi, S.; Ohta, Y.; Ishikawa, T. Structure-based approach for the discovery of pyrrolo[3,2-d]pyrimidine-based EGFR T790M/L858R mutant inhibitors. *ACS Med. Chem. Lett.* **2013**, *4*, 201–205.

(10) Gajiwala, K. S.; Feng, J.; Ferre, R.; Ryan, K.; Brodsky, O.; Weinrich, S.; Kath, J. C.; Stewart, A. Insights into the aberrant activity of mutant EGFR kinase domain and drug recognition. *Structure (Oxford, U. K.)* **2013**, *21*, 209–219.

(11) Yun, C.; Woo, M. S.; Greulich, H.; Meyerson, M.; Eck, M. J.; Wong, K. In *Structural and mechanistic studies of lung cancer mutations in the EGFR kinase reveal a novel mechanism of drug resistance*, 236th National Meeting of the American Chemical Society, Philadelphia, PA, Aug 17–21, 2008; American Chemical Society: Washington, DC, 2008; COMP 373.

(12) Davis, M. I.; Hunt, J. P.; Herrgard, S.; Ciceri, P.; Wodicka, L. M.; Pallares, G.; Hocker, M.; Treiber, D. K.; Zarrinkar, P. P. Comprehensive analysis of kinase inhibitor selectivity. *Nat. Biotechnol.* **2011**, *29*, 1046–1051.

(13) Yun, C.; Boggon, T. J.; Li, Y.; Woo, M. S.; Greulich, H.; Meyerson, M.; Eck, M. J. Structures of lung cancer-derived EGFR mutants and inhibitor complexes: Mechanism of activation and insights into differential inhibitor sensitivity. *Cancer Cell* **2007**, *11*, 217–227.

(14) Lovly, C. M.; Horn, L. Strategies for overcoming EGFR resistance in the treatment of advanced-stage NSCLC. *Curr. Treat. Options Oncol.* **2012**, *13*, 516–526.

(15) Ou, S. I. Second-generation irreversible epidermal growth factor receptor (EGFR) tyrosine kinase inhibitors (TKIs): A better mousetrap? A review of the clinical evidence. *Crit. Rev. Oncol. Hematol.* **2012**, *83*, 407–421.

(16) Miller, V. A.; Hirsh, V.; Cadranell, J.; Chen, Y.; Park, K.; Kim, S.; Zhou, C.; Su, W.; Wang, M.; Sun, Y.; Heo, D. S.; Crino, L.; Tan, E.; Chao, T.; Shahidi, M.; Cong, X. J.; Lorence, R. M.; Yang, J. C. Afatinib versus placebo for patients with advanced, metastatic non-small-cell lung cancer after failure of erlotinib, gefitinib, or both, and one or two lines of chemotherapy (LUX-Lung 1): A phase 2b/3 randomised trial. *Lancet Oncol.* **2012**, *13*, 528–538.

(17) Allen, L. F.; Eiseman, I. A.; Fry, D. W.; Lenehan, P. F. CI-1033, an irreversible pan-erbB receptor inhibitor and its potential application for the treatment of breast cancer. *Semin. Oncol.* **2003**, *30*, 65–78.

(18) Kalous, O.; Conklin, D.; Desai, A. J.; O'Brien, N. A.; Ginther, C.; Anderson, L.; Cohen, D. J.; Britten, C. D.; Taylor, I.; Christensen, J. G.; Slamon, D. J.; Finn, R. S. Dacomitinib (PF-00299804), an irreversible pan-HER inhibitor, inhibits proliferation of HER2-amplified breast cancer cell lines resistant to Trastuzumab and Lapatinib. *Mol. Cancer Ther.* **2012**, *11*, 1978–1987.

(19) Johnston, J. B.; Navaratnam, S.; Pitz, M. W.; Maniate, J. M.; Wiechec, E.; Baust, H.; Gingerich, J.; Skliris, G. P.; Murphy, L. C.; Los,

M. Targeting the EGFR pathway for cancer therapy. *Curr. Med. Chem.* **2006**, *13*, 3483–3492.

(20) Zhou, W.; Ercan, D.; Chen, L.; Yun, C.; Li, D.; Capelletti, M.; Cortot, A. B.; Chirieac, L.; Iacob, R. E.; Padera, R.; Engen, J. R.; Wong, K.; Eck, M. J.; Gray, N. S.; Janne, P. A. Novel mutant-selective EGFR kinase inhibitors against EGFR T790M. *Nature* **2009**, *462*, 1070–1074.

(21) Chang, S.; Zhang, L.; Xu, S.; Luo, J.; Lu, X.; Zhang, Z.; Xu, T.; Liu, Y.; Tu, Z.; Xu, Y.; Ren, X.; Geng, M.; Ding, J.; Pei, D.; Ding, K. Design, synthesis, and biological evaluation of novel conformationally constrained inhibitors targeting epidermal growth factor receptor threonine790 → methionine790 mutant. *J. Med. Chem.* **2012**, *55*, 2711–2723.

(22) Bai, F.; Liu, H.; Tong, L.; Zhou, W.; Liu, L.; Zhao, Z.; Liu, X.; Jiang, H.; Wang, X.; Xie, H.; Li, H. Discovery of novel selective inhibitors for EGFR-T790M/L858R. *Bioorg. Med. Chem. Lett.* **2012**, *22*, 1365–1370.

(23) Lee, H.; Schaefer, G.; Heffron, T. P.; Shao, L.; Ye, X.; Sideris, S.; Malek, S.; Chan, E.; Merchant, M.; La, H.; Ubhayakar, S.; Yauch, R. L.; Pirazzoli, V.; Politi, K.; Settleman, J. Noncovalent wild-type-sparring inhibitors of EGFR T790M. *Cancer Discovery* **2013**, *3*, 168–181.

(24) Zhou, W.; Ercan, D.; Chen, L.; Yun, C.; Li, D.; Capelletti, M.; Cortot, A. B.; Chirieac, L.; Iacob, R. E.; Padera, R.; Engen, J. R.; Wong, K.; Eck, M. J.; Gray, N. S.; Janne, P. A. Novel mutant-selective EGFR kinase inhibitors against EGFR T790M. *Nature* **2009**, *462*, 1070–1074.

(25) Merck Millipore Home Page. www.millipore.com.

(26) Singh, J.; Petter, R. C.; Baillie, T. A.; Whitty, A. The resurgence of covalent drugs. *Nat. Rev. Drug Discovery* **2011**, *10*, 307–317.

(27) Rauh, D. In *Targeting protein kinases with irreversible inhibitors*, 241st National Meeting of the American Chemical Society, Anaheim, CA, March 27–31, 2011; American Chemical Society: Washington, DC, 2011; MEDI 157.

(28) Singh, J.; Evans, E.; Hagel, M.; Labinski, M.; Dubrovskiy, A.; Nacht, M.; Petter, R. C.; Prasad, A.; Sheets, M.; StMartin, T.; Tjin Tham Sjin, R.; Westlin, W.; Zhu, Z. Superiority of a novel EGFR targeted covalent inhibitor over its reversible counterpart in overcoming drug resistance. *MedChemComm* **2012**, *3*, 780–783.

(29) Friesner, R. A.; Banks, J. L.; Murphy, R. B.; Halgren, T. A.; Klicic, J. J.; Mainz, D. T.; Repasky, M. P.; Knoll, E. H.; Shelley, M.; Perry, J. K.; Shaw, D. E.; Francis, P.; Shenkin, P. S. Glide: A new approach for rapid, accurate docking and scoring. 1. Method and assessment of docking accuracy. *J. Med. Chem.* **2004**, *47*, 1739–1749.

(30) Ehmke, V.; Quinsaat, J. E. Q.; Rivera-Fuentes, P.; Heindl, C.; Freymond, C.; Rottmann, M.; Brun, R.; Schirmeister, T.; Diederich, F. Tuning and predicting biological affinity: Aryl nitriles as cysteine protease inhibitors. *Org. Biomol. Chem.* **2012**, *10*, 5764–5768.

(31) Proteros Biostructures Home Page. www.proteros.de.

(32) Edwards, M. P.; Price, D. A. Role of physicochemical properties and ligand lipophilicity efficiency in addressing drug safety risks. *Annu. Rep. Med. Chem.* **2010**, *45*, 381–391.

(33) Leeson, P. D.; Springthorpe, B. The influence of drug-like concepts on decision-making in medicinal chemistry. *Nat. Rev. Drug Discovery* **2007**, *6*, 881–890.

(34) Leach, A. G.; Jones, H. D.; Cosgrove, D. A.; Kenny, P. W.; Ruston, L.; MacFaul, P.; Wood, J. M.; Colclough, N.; Law, B. Matched molecular pairs as a guide in the optimization of pharmaceutical properties; a study of aqueous solubility, plasma protein binding and oral exposure. *J. Med. Chem.* **2006**, *49*, 6672–6682.

(35) Johnson, D. S.; Weerapana, E.; Cravatt, B. F. Strategies for discovering and derisking covalent, irreversible enzyme inhibitors. *Future Med. Chem.* **2010**, *2*, 949–964.

(36) Clarke, E. D.; Greenhow, D. T.; Adams, D. Metabolism-related assays and their application to agrochemical research: Reactivity of pesticides with glutathione and glutathione transferases. *Pestic. Sci.* **1998**, *54*, 385–393.

(37) MacFaul, P. A.; Morley, A. D.; Crawford, J. J. A simple in vitro assay for assessing the reactivity of nitrile containing compounds. *Bioorg. Med. Chem. Lett.* **2009**, *19*, 1136–1138.

(38) Schwobel, J. A. H.; Madden, J. C.; Cronin, M. T. D. Examination of Michael addition reactivity towards glutathione by transition-state calculations. *SAR QSAR Environ. Res.* **2010**, *21*, 693–710.

(39) Esterbauer, H.; Zollner, H.; Scholz, N. Reaction of glutathione with conjugated carbonyls. *Z. Naturforsch., C* **1975**, *30*, 466–473.

(40) Bohme, A.; Thaens, D.; Paschke, A.; Schuurmann, G. Kinetic glutathione chemoassay to quantify thiol reactivity of organic electrophiles-application to α,β -unsaturated ketones, acrylates, and propiolates. *Chem. Res. Toxicol.* **2009**, *22*, 742–750.

(41) Paasche, A.; Schiller, M.; Schirmeister, T.; Engels, B. Mechanistic study of the reaction of thiol-containing enzymes with α,β -unsaturated carbonyl substrates by computation and chemoassays. *ChemMedChem* **2010**, *5*, 869–880.

(42) Krenske, E. H.; Petter, R. C.; Zhu, Z.; Houk, K. N. Transition states and energetics of nucleophilic additions of thiols to substituted α,β -unsaturated ketones: substituent effects involve enone stabilization, product branching, and solvation. *J. Org. Chem.* **2011**, *76*, 5074–5081.

(43) Gray, N. S.; Zhou, W. WIPO Patent WO2011140338, 2011.

(44) Tsou, H.; Mamuya, N.; Johnson, B. D.; Reich, M. F.; Gruber, B. C.; Ye, F.; Nilakantan, R.; Shen, R.; Discafani, C.; DeBlanc, R.; Davis, R.; Koehn, F. E.; Greenberger, L. M.; Wang, Y.; Wissner, A. 6-Substituted-4-(3-bromophenylamino)quinazolines as putative irreversible inhibitors of the epidermal growth factor receptor (EGFR) and human epidermal growth factor receptor (HER-2) tyrosine kinases with enhanced antitumor activity. *J. Med. Chem.* **2001**, *44*, 2719–2734.

(45) Serafimova, I. M.; Pufall, M. A.; Krishnan, S.; Duda, K.; Cohen, M. S.; Maglathlin, R. L.; McFarland, J. M.; Miller, R. M.; Froedin, M.; Taunton, J. Reversible targeting of noncatalytic cysteines with chemically tuned electrophiles. *Nat. Chem. Biol.* **2012**, *8*, 471–476.

(46) Bain, J.; Plater, L.; Elliott, M.; Shpiro, N.; Hastie, C. J.; McLauchlan, H.; Klevernic, I.; Arthur, J. S. C.; Alessi, D. R.; Cohen, P. The selectivity of protein kinase inhibitors: a further update. *Biochem. J.* **2007**, *408*, 297–315.

(47) Stamos, J.; Sliwkowski, M. X.; Eigenbrot, C. Structure of the epidermal growth factor receptor kinase domain alone and in complex with a 4-anilinoquinazoline inhibitor. *J. Biol. Chem.* **2002**, *277*, 46265–46272.

(48) Kabsch, W. Software XDS for image rotation, recognition and crystal symmetry assignment. *Acta Crystallogr., Sect. D* **2010**, *66*, 125–132.

(49) Emsley, P.; Cowtan, K. Coot: Model-building tools for molecular graphics. *Acta Crystallogr., Sect. D* **2004**, *60*, 2126–2132.

(50) Vagin, A. A.; Steiner, R. A.; Lebedev, A. A.; Potterton, L.; McNicholas, S.; Long, F.; Murshudov, G. N. REFMAC5 dictionary: Organization of prior chemical knowledge and guidelines for its use. *Acta Crystallogr., Sect. D* **2004**, *60*, 2184–2195.

(51) Gray, N. S.; Zhou, W. WIPO Patent WO2011079231, 2011.